Nature, timing and magnitude of buried Late Cretaceous magmatism on the central West Iberian Margin

Ricardo Pereira [1,2*], João Mata [2], Ricardo S. Ramalho [3,2,4,5], Filipe M. Rosas [2], Beatriz Silva [6], Patrícia Represas [7], Cláudia Escada [8]

[1] Partex Oil and Gas. Rua Ivone Silva, 6, 1st floor. 1050-124 Lisbon, Portugal. *Corresponding author. ricardo.pereira@partex-oilgas.com

[2] Instituto Dom Luiz (IDL), Faculdade de Ciências da Universidade de Lisboa, Campo Grande, 1749-016 Lisbon, Portugal.

[3] School of Earth and Environmental Sciences, Cardiff University, Park Place, Cardiff, CF10 3AT, UK.

[4] School of Earth Sciences, University of Bristol, Wills Memorial Building, Queen's Road, Bristol BS8 1RJ, UK

[5] Lamont-Doherty Earth Observatory, Columbia University, Comer Geochemistry Building, PO Box 1000, Palisades, NY10964-8000, USA.

[6] Departamento de Geologia, Universidade de Lisboa, 1749-016, Lisbon, Portugal

[7] Laboratório Nacional de Energia e Geologia (LNEG), Estrada da Portela, 2610-999 Amadora, Portugal.

[8] Departamento de Engenharia Geográfica, Geofísica e Energia, Faculdade de Ciências, Universidade de Lisboa, Campo Grande, 1749-016, Lisbon, Portugal

Keywords: Late Cretaceous alkaline magmatism, West Iberian Margin, Fontanelas volcano, sills, lava flows.

Abstract

The magma-poor West Iberian Margin, as part of the Peri-Atlantic alkaline province, records multiple evidence for intra-plate post-rift magmatism. Based on high-resolution multichannel seismic data, this work discusses the presence of large volcanic and intrusive features in the Estremadura Spur, providing evidence for important magmatic activity during the drifting of the continental margin. Our observations reveal distinct voluminous fissure-fed effusive sequences and the details of the 2800 m-high Fontanelas compound volcano, including its external and internal architecture, secondary vents and associated lava flows, all of which were probably extruded at intermediate water depths. Numerous and morphologically diverse sills and sill complexes are also described, attesting to the presence of a Late

Cretaceous shallow magmatic plumbing system in the area. Magmatism in this region is interpreted as having occurred during two main pulses and types of activity: 1) Coniacian to lower Campanian(?) age, characterized by fissural and fault-controlled volcanism, which mostly extruded massive lobate/sheet lava flows; and 2) a second voluminous intrusive and extrusive event of mid to late Campanian age, which includes the intrusion of the Estremadura Spur laccolith and the prominent Fontanelas compound volcano with associated dendritic lava flows. The inferred volumes of the first fissure-fed effusive event suggest a large eruption magnitude, comparable to some of the largest historical effusive eruptions. The second magmatic pulse led to the emplacement of discrete clusters of sills and sill complexes, as well as the construction of the ~2.8 km-high Fontanelas volcano, suggesting a syn-rift structural inheritance that controlled the location of the Estremadura Spur Intrusion and the Fontanelas volcanic area. Altogether, a total volume of rock exceeding 1.452 km^3 is estimated to have been emplaced or extruded in this region in a relatively short period, attesting to the prominence of the magmatism in this sector of the West Iberian Margin.

1. INTRODUCTION

Rifting events are often associated with magmatism, which either induced the stretching process by Rayleigh-Taylor instability of the sub-lithospheric mantle (active rifting) or resulted from adiabatic decompression consequence of far-field-induced lithosphere extension (passive rifting) (e.g. Huismans *et al.*, 2001; Geoffroy, 2005). On rifted continental margins, either rich or poor in their magma input, the role of magmatic events are consistently acknowledged to influence to different degrees, the margin's thermal state, eventually leading to breakup and subsequent rebound (e.g. Pérez-Gussinyé *et al.*, 2006; Leroy *et al.*, 2008; Franke, 2013). Additionally, magmatism can also affect fluid flow or the maturation and extent of any potential petroleum systems (e.g. Smallwood and Maresh, 2002; Bischoff *et al.*, 2017; Senger *et al.*, 2017; Mark *et al.*, 2018; Jackson *et al.*, 2020).

Lately, developments in the investigation of ancient magmatism on passive continental margins worldwide, with examples from the North Sea (Planke *et al.*, 2017; Walker *et al.*, 2020), New Zealand (Bischoff *et al.*, 2019), northwest and south Australia (Magee *et al.*, 2013; Magee *et al.*, 2017), and the South China Sea (Sun *et al.*, 2019), have revealed multiple records of buried volcanism and their associated plumbing systems. Such occurrences are thus recognized as usual characteristic of magma-rich rifted margins, in which plumbing systems are often linked to the period leading to lithospheric rupture and the onset of seafloor spreading, although occasionally persisting up to 10 Ma after breakup (e.g. Jackson *et al.*, 2013; Zhao *et al.*, 2016; Planke *et al.*, 2017).

The magma-poor and hyper-extended continental margin of West Iberian (Fig. 1), located in the transition from the central to northern Atlantic provinces, exhibits evidence for three

distinct magmatic cycles, in which the first two (at ca. 200 Ma and 148-140 Ma, respectively) are associated with two important extensional events during the rifting period and a third post-rift cycle of Late Cretaceous age of more uncertain origin (Manatschal, 2004; Martins *et al.*, 2008; Bronner *et al.*, 2011; Mata *et al.*, 2015).

This latter cycle postdates lithospheric breakup by ~ 30 Ma., being thus an example of intra-plate post-rift magmatism on the extended continental margin. Magmatic occurrences are well documented onshore (Fig. 2), including Upper Cretaceous magmatism widely distributed in central and south Portugal (Alves, 1964; Wright, 1969; Sparks and Wadge, 1975; Aires-Barros, 1979; Alves *et al.*, 1980; Rock, 1982; Bernard-Griffiths *et al.*, 1997; Miranda *et al.*, 2009; Grange *et al.*, 2010) (Fig. 1). In the Estremadura Spur several other offshore occurrences of intrusive and extrusive magmatic rocks has been described or suggested by geophysical potential field methods (Silva *et al.*, 2000; Neres *et al.*, 2018; Escada *et al.*, 2019), as well as by seismic studies, which unveilled a sizeable intrusion assigned to this same (Pereira *et al.*, 2017; Pereira and Barreto, 2018; Pereira *et al.*, 2021). Dredges on the offshore Fontanelas volcano revealed that the characteristics are akin of those depicted by the onshore late Cretaceous magmatism in the neighbouring Lisbon region (Miranda *et al.*, 2010). This magmatic cycle on the West Iberian Margin (WIM) is part of a vast intra-plate magmatic alkaline province that spreads out from the continental margin towards the oceanic domain, in which multiple other intrusions and volcanic buildings have been identified (Matton and Jébrak, 2009; Grange *et al.*, 2010; Merle *et al.*, 2018; Merle *et al.*, 2019). However, even on the neighbouring of the Iberia coastline, the offshore extension of this magmatism, their exact geometry, distribution and origin are still unclear, hampering our complete scientific understanding of the geodynamic evolution and its integration within the overall context the Atlantic.

This work primarily provides new insights on the post-rift magmatism affecting the offshore central WIM during the Late Cretaceous, by investigating high-resolution 2D and 3D seismic datasets (Fig. 1). This allowed an accurate morphological characterization of the magmatic features in the area, including evidence for vigorous volcanic and widespread intrusive activity. Critically, this study reveals new data for the Fontanelas volcanic edifice, providing a crisper image of its shallow plumbing systems and extrusive flows. This paper also aims to address the following key scientific questions: 1) What is the nature of the magmatic activity on the offshore WIM? 2) How many magmatic events can be recognised? and 3) What is the magnitude of this event?

2. GEOLOGICAL SETTING

The WIM, developed during the stretching events leading to the opening of the Atlantic Ocean, is one of the most well described hyper-extended passive margins in the world and

constitutes a type-example of a magma-poor domain (e.g. Manatschal, 2004; Pérez-Gussinyé *et al.*, 2006; Franke, 2013). Despite the limited magmatic input, magmatism on the WIM is recorded in three main events separated by circa 50 Ma, each associated with distinct phases of the evolution of the Iberian-Newfoundland conjugate margin (e.g. Mata *et al.*, 2015 and references therein): I) the latest Triassic to earliest Jurassic event (Verati *et al.*, 2007), which is part of the Central Atlantic Magmatic Province, exhibiting tholeiitic characteristics, negative εNd_i and radiogenic (>0.7050) initial Sr isotope ratios (Martins *et al.*, 2008; Callegaro *et al.*, 2014); II) Tithonian-Berriasian (148-140 Ma; Grange *et al.*, 2008; Mata *et al.*, 2015) rift-related mildly alkaline dykes with $+1.6 < \varepsilon Nd_i < +4.2$ and initial Sr isotope ratios close to the $CHUR_{145}$; and III) a post-rift alkaline cycle of Late Cretaceous age (98-69 Ma) (Fig. 2), exhibiting $\varepsilon Nd_i > +5$ and initial Sr isotope ratios assigned to a sub-lithospheric mantle source with a time-integrated evolution characterized Rb/Sr ratios noticeably lower than the CHUR (Miranda *et al.*, 2009; Grange *et al.*, 2010). With time, magmas become more enriched in incompatible elements, whilst their sources were progressively characterized by a lower $^{87}Sr/^{86}Sr$ but higher $^{143}Nd/^{144}Nd$ ratios and presenting elemental characteristics indicative of increasing depth of magma segregation (Mata et al., 2015). The post-rift cycle has geochemical characteristics compatible with a sub-lithospheric source, with the influence of a plume having been invoked (Grange *et al.*, 2010; Merle *et al.*, 2019). Such plume (*s.l.*) was recently considered as one of the mantle's upwellings zones anchored at the Central East Atlantic Anomaly, ponded below the 660 km anomaly (Civiero *et al.*, 2021).

This third cycle is the most significant and widespread magmatic event on the Iberian margin (Fig. 1), testified by multiple exposed manifestations of extrusive and intrusive activity, on the Central and Southern parts of Portugal, with the known radiometric ages pointing to two distinct pulses (94-88 Ma and 75-69 Ma) of magmatism (Miranda *et al.*, 2009). However, some discrepancy with paleomagnetic data has been noticed suggesting that some of the older geochronology results (namely those using K-Ar) should be revaluated (Neres *et al.*, 2018). These occurrences include the sub-volcanic alkaline intrusions of Sintra, Sines and Monchique, with multiple suites of granites, syenites, gabbros and nepheline syenites (78-71 Ma., K-Ar, Rb-Sr and U-Pb) (e.g. Alves, 1964; Wright, 1969; Sparks and Wadge, 1975; Rock, 1982; Miranda *et al.*, 2009; Grange *et al.*, 2010). In addition, effusive and explosive sequences are described in the Lisbon Volcanic Complex (LVC) (~73 Ma, K-Ar) composed of basaltic pyroclastic successions, lava flows and remnants of volcanic feeders (Alves *et al.*, 1980; Ramalho *et al.*, 1993; Miranda *et al.*, 2009), along with multiple dykes and sills, from which the Lomba dos Pianos, Paço de Ilhas (~88 Ma, K-Ar) or the Foz da Fonte (~94 Ma, Ar-Ar) are the most expressive examples (Miranda *et al.*, 2009; Neres *et al.*, 2014) (Fig. 1). In southern Portugal, several other manifestations can be observed, with multiple dykes, with ages up to

69 Ma (Grange *et al.*, 2010), crosscutting the Cretaceous sequence (see also Miranda *et al.*, 2009, and references therein). In addition to these observations, multiple magnetic anomalies tentatively assigned to magmatic intrusions of this same cycle have been recently investigated as part of the wider evidence of the extension of this province. Among these, the most prominent corresponds to the Estremadura Spur Intrusion (ESI) and the Guadalquivir-Portimão intrusion (Neres *et al.*, 2018; Escada *et al.*, 2019; Simões *et al.*, 2020), which bear implications on the sourcing, processes and distribution of sub-lithospheric igneous material in the central to north Atlantic region (Grange *et al.*, 2010; Merle *et al.*, 2019).

The Estremadura Spur, located on the central WIM and offshore the Lisbon region, is an uplifted hinge zone, bounded by two perennial first-order strike-slip zones, the Tagus and the Nazaré Fault Zones, both of which have played a major role in segmenting the WIM (Fig. 1) (Alves *et al.*, 2009; Pereira *et al.*, 2017). Here, the Late Cretaceous strata are strongly deformed as a result of NE-SW shortening of the margin during the Campanian-Early Paleocene, which resulted in generalised folding and reverse faulting, ultimately crosscut by a regional unconformity of Maastrichtian-Danian(?) age (Martín-Chivelet *et al.*, 2019; Pereira *et al.*, 2021). Tectonic inversion resumed in the Tertiary with two main pulses of shortening, by the mid-Eocene and Oligo-Miocene, recording the progressive rotation of the stress field towards a NW-SE direction that ultimately shaped the current geometry of the drifting margin. Deformation in the Estremadura Spur is also affected by the emplacement of a voluminous laccolith exceeding 942 km^3 (the ESI in Escada *et al.*, 2019; Pereira *et al.*, 2021). This is similar to the Sintra intrusion, where folds and associated ring to radial dykes, and sills that can be observed on outcrops (Alves, 1964; Ramalho *et al.*, 1993; Kullberg and Kullberg, 2017; Terrinha *et al.*, 2017). The ESI becomes evident on geophysical potential field anomalies, including free-air gravimetric anomaly exceeding 50 mGal and a total magnetic field (IGRF removed) of 90 nT, and on high-resolution seismic datasets (Escada, 2019; Escada *et al.*, 2019).

Dredge samples collected at the exposed top of the Fontanelas volcano revealed a suite of alkaline lava flows (mostly pillow lavas and hyaloclastites) ranging from foidite to alkaline basalt and assigned to a sub-lithospheric mantle source (Miranda *et al.*, 2010). According to the same authors, despite the lack of radiometric ages, but based on the geochemical signatures, the Fontanelas volcano is considered to be part of the same Late Cretaceous alkaline cycle observed onshore.

3. DATA AND METHODS

The analysis of the distinct magmatic features on the central WIM was accomplished by interpreting different exclusive datasets of high-resolution seismic surveys, that include 2D Two-Way Time (TWT) Post-Stack Time Migrated and 3D Pre-Stack Depth Migrated (PSDM)

seismic (Fig. 1). Seismic data was processed with zero phase and interpreted using normal polarity according to the standards of the Society of Exploration Geophysicists, where an increase in acoustic impedance corresponds to a positive red reflection and a decrease in acoustic impedance is displayed in black.

The estimation of seismic resolution of sills and lava flows, in the absence of any direct measurements or calibration, was achieved by considering a single velocity value of 5500 m/s, an approximation similar to values published in literature (e.g. Bartetzko *et al.*, 2005; Magee *et al.*, 2015). Considering the range of dominant frequencies at the interval of interest, of ~25 Hz, here estimated as a function of ~1/4 of the wavelength, the dataset allows to resolve igneous features of around 55 m thick. Despite the limitations on seismic resolution in resolving some of the thinner igneous features, that may be affected by tuning effects, obtained values are considered suitable for an overall analysis of its dimensions and the intruded rock volumes.

The recognition of sills on seismic data is usually accomplished by the visual identification of strong reflectivity features that contrast with the surrounding sediments, which can display a variety of forms and stratal relationships (e.g., planar, saucer-shaped, transgressive or combinations of these) (e.g. Planke *et al.*, 2005; Schofield *et al.*, 2012; Jackson *et al.*, 2013; Planke *et al.*, 2015). Moreover, as result of magma injection into pre-existing sedimentary deposits, sills are often associated with forced folding of the overlying strata, allowing to estimate the approximate age of magma emplacement at depth (Jackson *et al.*, 2013; Magee *et al.*, 2017; Niyazi *et al.*, 2021a).

The vertical thickness of the individual sills was obtained directly from the PSDM seismic volume in depth domain, by mapping the top and base reflections, and by measuring a single value at the apparent thickest point. This value was later multiplied by its calculated area to provide a notional volume of emplaced magma of the sills.

The volumes for individual lava flows were obtained with Petrel interpretation software, by visually filtering the 3D volume and generating geoprobes that highlight the very-high amplitudes from the PSDM seismic, in depth domain. Subsequently, the geoprobes were converted to individual 3D geobodies, each providing the output of an approximate rock volume that allow estimating a total volume of these lava flows.

In order to constrain the nature and any relations of extrusive features with neighbouring volcanic edifices, as well its implications on the investigation of the magmatic cycle, lava flows interpreted in this work are compared with examples observed in distinct geographical and magmatic settings (Thomson, 2004; Planke *et al.*, 2017; Reynolds *et al.*, 2017b; Sun *et al.*, 2019; Bischoff *et al.*, 2020). Aiming to investigate the internal structure, build-up mechanisms of the Fontanelas volcano and its implication for constraining the style of volcanism, a

comparison is established with previously documented buried volcanic edifices worldwide (Magee *et al.*, 2013; Reynolds *et al.*, 2017a; Bischoff *et al.*, 2019; Sun *et al.*, 2019).

In the absence of any direct correlation with boreholes in the submerged area, seismic stratigraphy criteria were used to characterize the distinct depositional mega-sequences (sensu Hubbard *et al.*, 1985). In parallel, relative age constrain of the identified magmatic features and associated sedimentary deposits was underpinned by regional geological information of the main depositional strata in which coeval magmatism is described (Witt, 1977; GPEP, 1986; Azerêdo *et al.*, 2003; Rey *et al.*, 2006; Alves *et al.*, 2009; Miranda *et al.*, 2009; Pereira *et al.*, 2021).

4. RESULTS

In this section new evidence is presented for the occurrence on the offshore the central WIM of distinct Late Cretaceous magmatic manifestations and their plumbing systems (Fig. 1). This includes the detailed analysis of numerous sills intruding this segment of the margin, the description of a large volcanic edifice (the Fontanelas Volcano) with evidence of secondary volcanic features, and its associated lava flows.

4.1. SILLS

One of the key testimonies of this magmatic event is the presence of multiple sills that were previously reported in the region (Pereira and Barreto, 2018; Simões *et al.*, 2020; Pereira *et al.*, 2021), although incompletely described and assessed for its significance; this is better accomplished in this study, which entails the clarification of some of these aspects.

On the Estremadura Spur region numerous sills and sill complexes can be identified on 3D seismic (Figs. 3, 4 and 5), and on outcrops (Fig. 6), from which 120 seismic features were investigated in detail for this study, namely by performing the analysis of their geometry, relative age and areal distribution. Characterised by high amplitudes on seismic data (Figs, 4, 5 and 7), predominantly intruding the unconformity-bounded sequence 5b (Turonian to mid-Campanian age, Fig. 2), sills are mostly of layer parallel to slightly saucer-shaped type showing on average 25-30 m thick intrusions (maximum of ~70 m) and an area of about 5 km^2, with the largest one reaching 59 km^2. These dimensions are comparable to what is observed in one of the best exposed examples of sills on onshore outcrops, the basalts of the Lomba dos Pianos sill (30-40 m thick), observed on a shoreline cliff located north of the Sintra massif (Figs. 1 and 6A-C). Despite the widespread distribution in the study offshore area, three main clusters of sills can be identified, namely in the vicinity of the Fontanelas Volcano, the ESI and in a central area in between the two (Figs. 3 and 4). The depth of sill emplacement commonly corresponds to 250-500 m below the base of seismic sequence 5c. However, a

more detailed analysis on the depth and timing of emplacement is hindered by the strong deformation and erosion of the stratigraphic boundaries.

In the area of the Fontanelas Volcano a group of at least 19 sills can be observed (Fig. 3). Some form sill complexes, while others occur isolated around the perimeter of the volcanic edifice, revealing a dominant layer parallel to slightly saucer shape geometry.

A cluster of over 15 sills of dominant layer parallel geometry can also be observed in the central area of the survey (Fig. 5A). Here, an outstanding ~15 km^2 slightly saucer shape sill (approximately 30 m thick, intruding unit 5b) exhibits evidence for forced folding and faulting of overlying strata (Fig. 7A-B). Folding is marked by an unconformity overlain by onlaps of depositional unit 5c, which ultimately provides constraints to the age of emplacement. South of Lisbon, the onshore Foz da Fonte dolerite sill (98±3.9 Ma; Miranda *et al.*, 2009) intrudes Albian strata (Fig. 6F), an example described in detail by Kullberg and Kullberg (2017), providing one of the few documented cases on outcrop to suggest evidence of forced folding.

Sills associated with the ESI stand out both atop the laccolith or around it, as highly reflective amplitudes (Fig. 5A and 5C). Despite issues in seismic imaging mainly due to limited acquisition and/or processing parameters, sills in this area are dominated by layer parallel and slightly saucer shaped, although in this region a few clear planar transgressive sills can be identified. In this area, a sill complex including an elongated 27 km^2 sill (maximum length of 9 km and 5 km wide, and about 40 m thick) (Fig. 7C-D), with slightly saucer shape geometry, also showing a peculiar pedunculate to concave shape, is interpreted to represent the locus of the feeder system associated to this cluster of intrusions, below which, some dimming of seismic reflections and postulated faults occurs, possibly revealing the presence of magma conduits. Analogue magmatic features can be observed on outcrop of the Sintra laccolith with multiple crosscutting dikes and sills of trachytic-basaltic nature (Alves, 1964; Ramalho *et al.*, 1993) (Fig. 6D-E). Similar examples are also interpreted on seismic sequences of the Rockall Trough, showing sill clusters associated with an intrusion (Archer *et al.*, 2005).

Notwithstanding some limitations in the interpretation of some magmatic features and the incomplete coverage of the Estremadura Spur area, an estimation of the intruded rock volume points to an approximate value in excess of 180 km^3 for the total number of mapped sills.

4.2. THE FONTANELAS VOLCANIC EDIFICE

The Fontanelas volcano stands out on bathymetry surveys as a 500 m-tall physiographic feature on the otherwise smooth recent sediment covered seafloor (Miranda *et al.*, 2010) (Fig. 3). Here, we present the details on both external and internal architecture of the volcanic edifice (Figs. 3, 9 and 10), aiming to later clarify the nature of the extrusive event, and ultimately to address the implications for the understanding of the magmatic cycle in West Iberia and the Atlantic.

4.2.1. EXTERNAL ARCHITECTURE OF THE VOLCANO

The analysis of the external morphology of the Fontanelas volcano was performed by mapping the top and base of the edifice both on 2D TWT and 3D PSDM seismic datasets. Overall, the geometry of the volcanic edifice reveals the presence of two distinct summits, although without clear evidence for craters or calderas (Figs. 8, 9 and 10). This is interpreted as a structural feature of the magmatism responsible for the build-up of the volcano rather than post-eruptive erosion, given that well-developed diatremes would be visible in the seismic structure of the edifice, if they were present. The overall morphology of the Fontanelas volcanic edifice is, nevertheless, eroded to some extent.

The general geometry of the Fontanelas reveals that it extends over a basal area of 500 km^2, with its shape characterised by an ellipsoid NE-SW trend, with approximate dimensions on the longer axis of about 30 km (Length, L) and 25 km (Width, W) on the shorter segment (Fig. 8). Based on the 2D mapping of the top and bottom of the volcanic edifice, a base-case isochron TWT thickness map was calculated, by applying an approximate interval velocity for basaltic rocks of 5500 m/s. Accordingly, we estimated the total height (H) of the volcano, which is of up to 2800 m (Fig.8). Nonetheless, acknowledging uncertainty of our estimations, or possible variations on the overall properties of the volcanic edifice (see Magee *et al.*, 2015 for the discussion on rock properties, and references therein), the total height could vary from 2250 m (using a velocity of 4000 m/s) to 3350 m (using 6000 m/s). This base-case analysis allows estimating some notional aspect ratios such as ellipticity (L/W) of 1.2 and a Height *vs* Length ratio (H/L) of ~0.09, which can be broadly compared in terms of its morphology to present-day polygenetic composite volcanoes (e.g. Grosse *et al.*, 2012; Grosse *et al.*, 2013), despite some limitations that allow comparing recent and ancient volcanoes . Moreover, based on the interpreted top and base of the edifice, an approximate total rock volume of 327 km^3 was calculated, which compares with other examples worldwide (Silva and Lindsay, 2015) and can fit to the category of shield to composite volcanoes, both in terms of the H/L ratio and rock volume. These aspects combined, can be used later to assess the nature of volcanism and its implications.

In order to investigate the conditions in which the volcano originated, namely for the sub-aerial or submarine paleo-topographic controls, we compared our data with buried volcanoes on the northern South China Sea (Sun *et al.*, 2020), in which typical hydromagmatic volcanic edifices extruded under shallow water conditions. In contrast to the features described by these authors, the Fontanelas Volcano does not exhibit evidence of a well-developed diatreme.

4.2.2. INTERNAL ARCHITECTURE AND VOLCANIC PLUMBING SYSTEM

Similar to descriptions of other buried volcanoes worldwide (e.g. Bischoff *et al.*, 2017; Bischoff *et al.*, 2019; Walker *et al.*, 2020), the internal structure of the Fontanelas volcano reveals multiple outward-dipping reflections, interpreted to express the progressive growth of the edifice (Fig. 9). Underlying the volcano, the seismic signal is characterised by noisy to very discontinuous reflectors and dimmed amplitudes, which is interpreted as resulting not only from seismic signal attenuation from the volcanic edifice itself, but also as likely revealing a sub-vertical plumbing system. Comparable to other buried volcanic edifices (Bischoff *et al.*, 2017; Niyazi *et al.*, 2021a), despite the limited resolution, a similar volcano architecture is expected in which, several high amplitude reflectors can be observed. Reduction of seismic resolution is likely the indirect evidence of an underlying complex feeder system, comprising not only the observed sills, but also elusive conduits, stocks or previous magma reservoirs.

4.3. LAVA FLOWS

Associated with the Fontanelas volcano, two main groups of high seismic amplitude features are identified and strongly contrasting with surrounding strata (Figs. 3, 8, 10 and 11; Table 1). At first sight, they that can be compared either with magmatic extrusive examples (Planke *et al.*, 2017; Reynolds *et al.*, 2017b; Sun *et al.*, 2019) or with sill morphologies (Thomson and Hutton, 2004; Schofield *et al.*, 2012; Magee *et al.*, 2017).

The first group includes five high-confidence features that are observed within stratigraphic unit 5b (lava flows LF1 to LF5), dominantly along a continuous seismic reflector in which, the distinct reflective bodies are laterally overlapping (Fig. 10). Detailed interpretation and seismic amplitude extraction of each of these features reveals that they form individual elongated and adjoined fan-like geometries clearly showing lobes with crenulated margins (Fig. 11A-E). Although some of these morphological features share similarities with large sills, they lack some of the key criteria that are typical of these intrusive entities, like cross-cutting strata or their generally lower aspect ratio (length/width) translated in more sub-circular to elliptic shape (e.g. Schofield *et al.*, 2012). Contrastingly, these seismic features are closely comparable to lava flows described in the Atlantic North Sea or the South China Sea (Planke *et al.*, 2017; Sun *et al.*, 2019). Accordingly, the interpreted features often reveal multiple elongated geometries indicative of several events of nearly synchronous flow, forming fans along a similar path of extrusion, likely controlled by pre-existing topography (see lava flows LF1, LF2 and LF3, Figs. 11A, B and E). Lava flow 3 (Fig. 10C), however, is characterised by a sheet-like geometry with some lobate marginal crenulation and shows an irregular path, changing from a westward direction of flow, towards a NW trend. Despite its distinct geometry, the trajectory apparently shares a common vent with lava flows 1 to 4 (Fig. 11 and 12). This group of pre-Fontanelas extrusive features points to a postulated location for extrusion that seems

related with a group of faults, likely inherited from the syn-rift extensional phase, later reworked during inversion, as expressed by noteworthy tilting and folding of the late Cretaceous strata, sills and the lava flows (Fig. 12). This common rooting, as well as their exact same stratigraphic position, thus strongly suggest these lava flows were extruded during the same eruptive event.

Lava flow 5, characterised by two individual and sub-parallel fan shape geometries, is overall smaller in area and volume (Figs. 8 and 11E). LF5 is observed to overlay LF2, suggesting that it is relatively younger than the former extrusive sequence (Fig. 10). Despite, showing a distinct SW direction of flow when compared with the other lava flows (LF1-4), suggesting that an alternative source of extrusion may have been present, LF 5 is considered as part of the same extrusive event.

Aiming to obtain an approximation of the expelled volume of rock for pre-Fontanelas extrusive event (Lava flows LF1 to LF5, Table 1), extraction of geoprobes (a 3D rendering tool based on the extraction of high seismic amplitudes) for each lava flow was performed. This approach indicates that altogether these features comprise a total of 2.7 km^3 of magma that was extruded during this event and for this location. This is an approximate value given this analysis does not account for all possible lava flows imaged by seismic data, the time-depth conversion uncertainties associated with the final PSDM seismic volume,

A second group of seismic high-amplitude features is directly associated with the base and top boundary of the volcano (lava flows LF6 to LF8), which is stratigraphically distinct (and younger) than the lava flows described above. These features have a clear dissimilar shape relatively to those previously described, with its seismic features revealing dendritic and sheet-like geometries (Fig. 11F-H). These are characterised by high amplitudes with very elongated channelised features, typically forming dendritic lobes at its terminations and interpreted here as lava flows, in which the source can be tracked to the volcanic edifice itself. Lava flows LF6 and LF7 are interpreted at the base of the volcanic edifice, whereas lava flow LF 8, located in the flank is associated to one of the latest extrusive events. The relative stratigraphic position and geometry of these lava flows contrasts with those described previously, which bears implications on the type of volcanism under analysis in each case (see discussion below).

5. DISCUSSION

West Iberia records multiple events of intra-plate magmatism, in which, the so called Late Cretaceous alkaline cycle is often considered as part of a larger magmatic province that extends throughout the peri-Atlantic domain (e.g. Matton and Jébrak, 2009; Miranda *et al.*, 2009; Grange *et al.*, 2010; Merle *et al.*, 2019). Adding to this understanding, new evidence from the subsurface, including its tectono-magmatic insights, helped to bring forward an updated view on the larger extent, significance and implications on this cycle (Pereira *et al.*,

2017; Neres *et al.*, 2018; Pereira *et al.*, 2021). Building on our new observations, that include the details on the presence a large volcanic edifice (the Fontanelas Volcano), along with lava flows and also, numerous sills and sill complexes, as part of a complex magmatic plumbing system, a discussion is herein presented, aiming to elaborate on the type, timing and magnitude of magmatism, as well as the implications for the wider WIM magmatic province, as a whole.

5.1. ASSESSING THE TYPE OF MAGMATISM

In the absence of any direct methods to investigate the buried Late Cretaceous magmatic activity on the Central WIM, the type of magmatism is here discussed based on seismic geomorphology observations. It is also compared to evidence of ancient plumbing systems (either cropping out on the onshore WIM or to other regions imaged by seismic reflection methods), as well with examples from extant volcanic regions worldwide.

The analysis of the sills and sill complexes intruding this segment of the margin shows that these are mainly distributed in three domains, namely, 1) in the vicinities of the ESI; 2) the Fontanelas volcano; and 3) at a central area in between these two entities. Based on the fault pattern and the location of the intrusions (Fig 4), the clustering of sills is interpreted to have been controlled by pre-existing structural weaknesses inherited from the previous sin-rift tectono-sedimentary evolution, which would favour distinct areas for magma ascent and emplacement. The role of structural inheritance controlling the magma emplacement in the Lusitanian Basin, is also reported to Jurassic-Cretaceous transition dykes and sills, associated with multiple salt diapirs (Mata *et al.*, 2015; Davison and Barreto, 2021).

In the Estremadura Spur area, Late Cretaceous sills tend to be emplaced in areas where WNW-ESE reverse faulting is noticeable (Fig. 4). Here a group of reverse faults (Figs. 5B and 7A-B) are observed underlying the sills. Evidence of this tectonic imprint acting as conduits is also suggested by inclined seismic reflections underlying the ESI (feeder dykes?), as well as dimming of seismic data along with upward bending reflections underlying the Fontanelas volcano, as part of the wider plumbing system (Figs. 3, 5 and 9). Similar evidence on the detailed imaging of plumbing systems is discussed with examples from the southeast Australian Margin and the Faroe-Shetland region (McLean *et al.*, 2017; Niyazi *et al.*, 2021a; Niyazi *et al.*, 2021b). Accounting for the position of the sills in relation with the volcanic edifice and any controls from structural inheritance (McLean *et al.*, 2017; Barrier *et al.*, 2021; Niyazi *et al.*, 2021b), these igneous features are interpreted to be associated with underlying syn-rift faults; these faults probably acted as conduits for magma ascension to its final position within a pre-volcanic sequence (dominantly unit 5b) and in some cases, extruding to surface and contributing to the build-up of the volcanic edifice (Fig. 4). Another relevant aspect of sills in the vicinity of the ESI is the similarity to what is observed around the Sintra massif (Fig. 6D-

E) (Alves, 1964; Sparks and Wadge, 1975; Ramalho *et al.*, 1993). Sills are distributed both on top of the ESI laccolith and around it, what can be interpreted as being part of a similar complex network of ring and radial dykes.

The type of magmatism can be diagnosed in more detail by the analysis of its lava flows. Our observations allowed the discrimination of two groups of lava flows, with distinct location, geometries, and relative time of emplacement. A first group of lava flows (LF1–LF5, Fig. 11), pre-dating the build-up of the Fontanelas volcano, and observed south of the volcanic edifice, include fan- and lobate-shaped lava flows with crenulated lobate margins, extending on a kilometre scale towards the NW, support a distinct source from the main volcanic feeding system. These morphologies are very distinctive and are clearly akin to voluminous “inflated” sheet or 'a'ā lava flows extruded under high to very high effusion rates, such as those described in historical subaerial eruptions (e.g., at Hawaii Peterson and Tilling, 1980), at Fogo volcano, (Mata *et al.*, 2017), in Iceland (Planke *et al.*, 2017), or such as those described at deep-sea submarine eruptions on seamounts and mid-ocean ridges (e.g. Axial Seamount and East Pacific Rise; Chadwick Jr. *et al.*, 2013; White *et al.*, 2015). The root of these lava flows converges to the south of the volcanic edifice, suggesting that the vent that fed them may be located in this area, although not fully evident on seismic data. Moreover, the lack of a significant volcanic edifice at this exact stratigraphic level, as well as the convergence of the root of these flows along an elongated area, suggests that these lava flows resulted from a voluminous fissure-fed effusive eruption, alike those produced along the rift zones of Iceland (such as the 2018 Holuhraun eruption), in Afar (Ethiopia), or at the Axial Seamount, in the present day.

Assuming that this first group of lava flows (LF1-5) were extruded during a specific and relatively time-constrained eruption (as their common origin, geometry and stratigraphic position suggest) their combined volume amounts to 2.69 x 10^9 m^3, which is significant. If we consider a density ranging in 2600 to 2800 kg/m^3 for the basalts that compose these flows[1], this combined volume corresponds to a total extruded mass of 7.0–7.5 x 10^{12} kg, leading to an estimated eruption magnitude of 5.8–5.9 (as defined by Pyle, 2015). For comparison, these values are in the same range of some of the largest effusive eruptions (e.g., the June 1950 Mauna Loa eruption) registered in historical times, thus attesting to the very large size of the eruptive episode and its relative importance within the context of what is generally considered a magma-starved margin.

Considering this evidence, and since these fissural lava flows pre-date the build-up of the Fontanelas volcano, we interpret that these features constitute one of the first expressions of

[1] The bulk of the volume of thick or “inflated” submarine sheet or subaerial 'a'ā lava flows corresponds to the coherent, generally vesicle-poor interior/core, and therefore the density of such flows typically approximates the values for non-vesicular basalt.

463 magmatic extrusion in the area. Effectively, these lava flows attest to an earlier, dominantly
464 effusive, and highly voluminous fissure-fed eruptive phase of the Late Cretaceous magmatism
465 in this sector of the margin, here documented for the first time and a unique description for
466 ancient volcanic systems.
467 The second group of lavas, either at the base (depicting the first flows) or at the top flank
468 of the Fontanelas volcano, is directly associated with prolonged volcanic activity at this
469 eruptive vent. In contrast with the extrusive features described above, these lava flows are
470 characterised by an overall channelised/dendritic geometry forming lava lobes and digitations
471 at its terminations, characteristics that are typical of lava flows extruded under low effusion
472 rates. This morphology suggests an emplacement similar to that of present-day lobate
473 pāhoehoe flows or to submarine lobate flows (see Kereszturi *et al.*, 2015 and references
474 therein).
475 The morphology of the Fontanelas volcanic indicate the presence of two distinct
476 culminations, which along with its complex internal structuration (although not fully resolved
477 on 3D seismic data), suggests that this an example of a compound volcano, with two main
478 eruptive centres. This interpretation is reinforced by the presence of multiple vertical zones of
479 dimmed seismic reflectivity under each inferred volcanic centre, interpreted as volcanic feeder
480 conduits. Additionally, the evidence of distinct internal outward-dipping reflections in the
481 Fontanelas edifice, with these internal reflections not being parallel to the top surface of the
482 volcano, indicates that through time the edifice has grown to different shapes and by building
483 distinct layers, to ultimately reach its final architecture and size as a polygenetic volcano.
484 A fundamental question that is worth asking concerns the subaerial *vs.* submarine nature
485 of the described volcanic features/edifices. The answer to this question is not straightforward
486 and the different possibilities are worth discussing here. The morphology of the described lava
487 flows is both compatible with subaerial or deeper water features, but is not compatible with
488 shallow water volcanism. At shallow water environments (i.e. <150 m water depth), hydrostatic
489 pressures are low enough to allow for the production of large quantities of steam when the hot
490 magma contacts the water, resulting in either surtseyan or taalian eruptions (depending of the
491 water/magma ratio), both of which are violently explosive and lead to the generation of large
492 tuff cones and rings and well-developed diatremes (see Sheridan and Wohletz, 1981;
493 Verwoerd and Chevallier, 1987; Sohn, 1996; Sun *et al.*, 2019). These, however, are not
494 features observed at the Estremadura Spur. Conversely, both the Fontanelas volcano and the
495 lava flows sequence that precedes this edifice are dominantly effusive and lack large craters
496 and diatremes. It is therefore highly unlikely that these features were extruded under shallow
497 water conditions.
498 A subaerial origin for these features is possible – and to some extent appealing, given that
499 higher similarity of the described lava flows with other lava flows extruded on land, but poses

some challenges. Indeed, albeit being eroded at the crest, the overall morphology and internal structure of each of the individual volcanic edifices is compatible with largely subaerially-built polygenetic composite volcanoes. If so, the Fontanelas volcano and adjacent secondary vents would have been built by bimodal volcanism (explosive and effusive) in an essentially subaerial environment, with eventually some subaerially-extruded flows entering a shallow water environment at the foot of the volcano (if the lobate flows described above correspond to submarine flows and not pāhoehoe flows). This could be compared with evidence from outcropping features in the coeval LVC where the main subaerial volcanic deposits, including pyroclastic deposits interlayered with lava flows, are observed blanketing an unconformity cross-cutting upper Cenomanian limestones with rudists and carbonate conglomerates (Aires-Barros, 1979; Alves *et al.*, 1980; Marques *et al.*, 1998; Manupella *et al.*, 2011). In the Lisbon region, post-Cenomanian strata are absent, with the only preserved deposits described in the northern Lusitanian Basin and in the offshore (e.g. Witt, 1977; Rey *et al.*, 2006) (Fig. 2). Strata include fluvial-deltaic siliciclastic and shallow marine/transitional carbonates of Turonian to Maastrischtian age, suggesting that after a period of widespread margin exposure, shallow marine deposition resumed and progressively flooded the Estremadura Spur (sequence 5C), blanketing the exposed (?) volcanic edifice. The fact, however, that the described volcanic sequences are within a stratigraphic unit composed of limestones (Fig. 2), poses thus a paleoenvironment problem, requiring multiple sea-level oscillations to intercalate supposedly subaerial volcanic products with marine limestones.

The most likely scenario is thus, for the described volcanic sequences, to have been extruded in a submarine environment, at intermediate water depths, necessarily comprehended above the carbonate compensation depth and below the critical depth for the onset of hydromagmatic explosive volcanism (~150 m). This scenario is also supported by the fact that mafic pillow lavas and hyaloclastites were dredged from the top of the Fontanelas volcano (Miranda, 2010). In addition, the existence of possible erosional terraces at the flanks of the Fontanelas volcano (see Fig. 9), suggests that, despite the Tertiary strata blanketing the volcanic edifice, the edifice was possibly eroded posteriorly by marine erosion during sea-level oscillations. The edifice nevertheless constituted a significant landmark from the late Cretaceous to the Paleogene, when ultimately, a combination of relative sea-level rise, marine deposition and tectonism of the margin fully submerged and buried the Estremadura Spur under the transgressive sequence we see today.

5.2. TIMING OF MAGMATIC EVENTS

In the absence of age dating for the igneous rocks in this offshore area, the timing of magmatic events must be tentatively established based on the seismic-stratigraphic framework, underpinned by the regional setting. As a whole, and as shown in this study, the

timing of these magmatic activity is bounded between units 5a and 5c ranging from Turonian to Campanian (~94 to 72 Ma). This indicates that the reported magmatic activity should be considered as part of the third Mesozoic cycle of magmatic activity at the WIM, as already suggested by Miranda *et al.* (2009) for the Fontanelas volcano, based on its alkaline characteristics.

The analysis of the relative stratigraphic position of the distinct manifestations of magmatism in the Estremadura Spur suggest that two pulses of magmatic activity have occurred. Accordingly, the age constraint of the main magmatic events take into account: 1) the onlap-bounded unconformity of base unit 5c (of interpreted mid Campanian age), associated with the onset of the ESI intrusion and forced folding (Figs. 5 and 7); and 2) the Base Tertiary Unconformity (Maastrichtian-Danian?) (Fig. 2).

The first magmatic pulse is marked by the effusive event within sequence 5b, preceding the intra-Campanian unconformity, with the extrusion of voluminous lava flows (LF1 to LF5) (Figs. 10 and 11) fed by fissural volcanism. This means that the first magmatic event is consequently older than the onset of intrusion/extrusion of the ESI and the Fontanelas volcano. Considering these criteria, a tentative Coniacian to lower Campanian age (~ 90 to 84 Ma) for this initial event is considered, a period that can be compared with the first magmatic pulse also observed at outcrops (e.g., Lomba dos Pianos), but likely younger than the Foz da Fonte sill (93.8±3.9 Ma; Miranda *et al.*, 2009), the first documented and undoubtful example of the magmatic cycle onshore (Figs, 1, 2 and 6).

The second and more voluminous magmatic pulse can be positioned during the mid to late Campanian (~80 to 72 Ma), as it apparently slightly precedes the onlap of unconformity bounded unit 5c, with evidence of forced folding (Fig. 7), and includes the ESI laccolith, the Fontanelas volcanic edifice and most of the sills and sill complexes. Combined, these two interpreted pulses of magma in the Estremadura Spur are coeval with those (94-88 Ma; 75-72 Ma) observed onshore (Miranda *et al.*, 2009), thus providing significant assurance to our analysis.

5.3. MAGNITUDE OF MAGMATISM

To investigate the approximate magnitude of the combined magmatic event, partial rock volumes have been estimated, including the ESI laccolith, the high confidence sills, the Fontanelas volcano and its associated lava flows. Despite some limitations on the dataset and the methods allowing to quantify the different rock volumes, the estimated volumes of magmatic material are not an absolute value but provide an indication of the overall magnitude of the wider event. For the ESI laccolith intrusion, Pereira *et al.* (2021) report a total volume of 942 km^3. From the data obtained for this study, we estimate that the sills account for ~180 km^3 of intruded material, the Fontanelas volcano (including lava flows at base and top), has yielded

572 a base-case around 327 km^3 of rock (ranging from 250 to 380 Km^3). For the associated pre-
573 Fontanelas lava flows, the lower estimate points to an excess of 2.7 km^3 of extruded magma.
574 Altogether, considering the individual or groups of magmatic features, a total volume of
575 magma of 1452 km^3 is estimated to have been extruded/intruded at the Estremadura Spur,
576 on a total area of about 2500 km^2. These values, which are an absolute minimum estimate
577 (not excluding additional unresolved magmatic features in the area or others that may be
578 located outside the high-resolution 3D dataset, and not accounted herein), confirm that the
579 post-rift magmatism that took place at the WIM during the Late Cretaceous was indeed very
580 sizeable. This is more so, when the overall volume of pene-contemporaneous magmatism
581 found onshore is also considered.
582 This places the Late Cretaceous magmatism as a dominant event in the region, spreading
583 out over an area of 30.000 km^2 on the whole proximal WIM. This portion of the wider magmatic
584 province reveals clear implications in what concerns the thermal evolution of the margin and
585 its geodynamic context. Although limited by scarce data, evidence from petroleum systems
586 modelling and oil typing on the Porto and Lusitanian Basins (Beicip-Franlab, 1996; Ferreira,
587 2017) suggest that during this period the impact of a widespread and deep heat source may
588 have thermally controlled conditions for fluid flow in the continental crust.
589 The third cycle post-dated the lithosphere breakup by some 30 Ma (Miranda *et al.*, 2009
590 and references therein) and presents geochemical characteristics compatible with a dominant
591 asthenospheric signature (Miranda *et al.*, 2009; Grange *et al.*, 2010). Acknowledging the wider
592 expression and magnitude of Late Cretaceous alkaline intra-magmatism may condition the
593 view on the dominant processes controlling this event, whether related to mantle plume-
594 derived melting leading to the formation of “hotspots” on the margin (Oyarzun *et al.*, 1997;
595 Grange *et al.*, 2010; Merle *et al.*, 2019) or, alternatively, as the combined product of edge-
596 driven convection and continental insulation, that would have favoured magma ascent from a
597 shallow mantle source (e.g. Matton and Jébrak, 2009). Recent seismic tomographic data
598 (Civiero *et al.*, 2021) favours the plume model with several partially coeval mantle upwellings
599 (plumes, s.l.) explaining the abundance of Late-Cretaceous to Cenozoic intraplate magmatism
600 in a vast region of the Central East Atlantic. According to this study such plumes are anchored
601 at the Central East Atlantic Anomaly, ponded below the 660 km anomaly.

602 ## 6. CONCLUSIONS

603 The Late Cretaceous alkaline cycle on the central West Iberian Margin is revealed to
604 include the Fontanelas volcano with its associated lava flows and the multiple manifestations
605 of a shallow magmatic plumbing system, including numerous sills, and the Estremadura Spur
606 Intrusion.

Sills are characterised by multiple geometries that range from planar to saucer-shaped, (occasionally forming sill complexes), dominantly intruding 250-500 m below the top of unit 5B of mid-Campanian age. On average they are 30-40 m thick, with individual areas that can reach 59 km^2. These intrusive features are clustered in three main areas, an observation that suggests that its emplacement was largely controlled by inherited syn-rift faulting.

The analysis of both external and internal architecture of the Fontanelas volcano reveals that the volcanic edifice denotes a complex geometrical and extrusive evolution, marked by successive periods of growth, to ultimately form a two-summit stratovolcano reaching a total height of ~2800 m. Two distinct groups of lava flows are identified around the volcano, that include: 1) A cluster of five features of kilometre scale fan-shape to tabular crenulated submarine sheet or 'a'ā lava flows, that precede the build-up of the Fontanelas edifice, created by a large fissure-fed effusive eruption with an estimated magnitude of 5.8–5.9, comparable to the June 1950 Mauna Loa eruption.; and 2) Dendritic and lobate lava flows (either pahoehoe or submarine lobate flows) directly associated with the volcanic build-up. Accordingly, the Fontanelas volcano is interpreted to represent an example of a composite and compound volcanic edifice, possibly extruded at intermediate water depths comprehended above the carbonate compensation depth and below the critical depth for the onset of submarine explosive volcanism.

Magmatism on the central WIM is interpreted to have occurred during two main pulses: I) Coniacian-lower Campanian(?) age, marked by the extrusion of the first lavas under fissural volcanism; and II) the intrusion of the ESI, the Fontanelas volcano and most of the sills during mid-late Campanian.

With a total volume of magma involved in this system (from the ESI, Fontanelas, lava flows and sills) in excess of 1452 km^3, the Late Cretaceous magmatic event is shown to represent a sizeable event, both in extent and magnitude. This bears implications for the further understanding of the peri-Atlantic alkaline province and for controlling any fluid flow to charge prospective petroleum systems or by reducing crustal strength during tectono-magmatic events.

Acknowledgments

The authors wish to thank the support of Partex Oil and Gas, for allowing the wider research project to be implemented and for the permission to publish the data. R.R. acknowledges his IF/01641/2015 “Investigador FCT” contract, funded by Fundação para a Ciência e Tecnologia I.P (FCT). This work was supported by the project FCT/UIDB/50019/2020 - IDL funded by FCT.

Conflict of Interests

The authors declare that there is no conflict of interests.

Figures

Figure 1. Location of the area of interest showing the distribution of magmatism on the central West Iberian Margin. ESI – Estremadura Spur Intrusion, LVC – Lisbon Volcanic Complex, AF – Aveiro Fault, NFZ – Nazaré Fault Zone, TFZ – Tagus Fault Zone, PSF – Pereira de Sousa Fault, MPF – Marquês de Pombal Fault, MPFZ – Messejana-Plasencia Fault Zone.

Figure 2. Stratigraphic framework of the West Iberian Margin showing the distinct megasequences, lithostratigraphic units and evidence of the Late Cretaceous alkaline magmatism. LBS – Lithosphere Breakup Sequence (Unit 5a).

Figure 3. Seismic line (in depth) across the Estremadura Spur, showing the evidence of the Fontanelas volcano, the Estremadura Spur Intrusion with associated sills (red) and lava flows (purple), as part of the larger magmatic plumbing system of the Late Cretaceous. BTU – Base Tertiary Unconformity.

Figure 4. Map showing the location of the Fontanelas volcano, the dominant distribution of sills (red) and lava flows (purple), and the Estremadura Spur Intrusion (ESI).

Figure 5. Seismic lines (in depth) showing the distribution and different geometry of sills (in red) throughout the Estremadura Spur. Note that sills and sill complexes are dominantly emplaced within sequence 5b. Location of seismic lines in figure 4.

Figure 6. Outcropping examples of the Late Cretaceous magmatism. A) Lomba dos Pianos sill, as seen on Google Maps perspective, showing the relation between the Albian-Cenomanian limestones and marls. Approximate thickness of the sill is 30-40 m. Lat: 38°53'36.22"N, Long: 9°26'18.00"W. B) Detail of the Lomba dos Pianos sill showing the top contact with limestones, evidencing prismatic joints. View to the South. C) Detail of the basaltic sill, showing zeolites filling fractures. D) Crosscutting trachytic-basaltic(?) ring dykes associated with the Sintra intrusion, at Ponta da Abelheira. View to the South. Lat: 38°44'52.81"N; Long: 9°28'18.36"W. E) Trachytic-basaltic(?) dykes and sills crosscutting late Jurassic limestones at Ponta da Abelheira, showing the landscape of the Sintra massif at a distance. F) The Foz da Fonte sill intruding Albian limestones, an example of forced folding associated with shallow magma emplacement; Lat: 38°27'3.91"N, Long: 9°12'6.25"W.

Figure 7. Details of sills intruding the Estremadura Spur. A) Seismic section showing an example of a planar-slightly saucer chape sill intruding unit 5b, with forced folding and faulting of overburden strata, with onlaps at base of sequence 5c. Note faulting at the edge of sill, tentatively interpreted as conduit for magma emplacement. B) 3D view of the sill showing the flanks of the sill. C) Sill complex intruding unit 5b, highlighting the presence of a saucer-shape

sill and possible magma conduit. D) 3D view of the sill, showing it complex geometry and possible source of magma flow.

Figure 8. A) Thickness map of the Fontanelas volcanic edifice, based on 2D/3D seismic data, with associated lavas (1 to 8), with interpreted flow directions from a common source. Note the presence of secondary volcanic vents. B) TWT structural map of the Fontanelas volcano.

Figure 9. TWT seismic lines across the Fontanelas volcano, highlighting the internal structuration and build-up of the volcanic edifice (outward dipping reflectors), lava flows (in purple), associated secondary vents and deep plumbing systems with multiple sills (in red). Possible erosional terraces at the flank of the volcano suggest possible influence of submergence and shallow water conditions.

Figure 10. Random seismic line across the southern flank of the volcano, showing pre-Fontanelas lava flows (1 to 5) and syn-Fontanelas lava flows (6-8). See figure 8 for location, figure 11 and Table 1 for details of the lava flows.

Figure 11. Plan view of seismic amplitudes of interpreted flows, showing multiple lava fans, lobate to crenulated terminations. Arrows indicate likely direction of flow, in relation to its interpreted source and the position of the Fontanelas volcano.

Figure 12. 3D perspective (in depth) of pre-Fontanelas lava flows and interpreted source for fissural magmatism preceding the build-up of the main volcanic edifice. Note the confluence of the origin of lava flows onto inversion faults, likely inherited from the syn-rift architecture.

Table 1. Description and characteristics of the lava flows associated with the Fontanelas volcano.

Conflict of Interests

The authors declare that there no conflict of interests during this work nor for its publication.

References

Aires-Barros, L. (1979) Actividade Ígnea Pós-Paleozóica No Continente Português (Elementos Para Uma Síntese Críitica). *Ciências da Terra*, **5,** 175-214.

Alves, C.a.M. (1964) Estudo Petrológico Do Maçico Eruptivo De Sintra. *Revista da Faculdade de Ciências de Lisboa*, **XXII,** 124-289.

Alves, C.a.M., Rodrigues, A., Serralheiro, A. & Fria, F. (1980) O Complexo Basáltico De Lisboa. *Comunicações dos Serviços Geológicos de Portugal*, **66,** 111-134.

Alves, T.M., Moita, C., Cunha, T., Ullnaess, M., Myklebust, R., Monteiro, J.H. & Manupella, G. (2009) Diachronous Evolution of Late Jurassic-Cretaceous Continental Rifting in the Northeast Atlantic (West Iberian Margin). *Tectonics*, **28,** TC4003. 10.1029/2008TC002337.

719 Archer, S.G., Bergman, S.C., Iliffe, J., Murphy, C.M. & Thornton, M. (2005) Palaeogene
720 Igneous Rocks Reveal New Insights into the Geodynamic Evolution and Petroleum
721 Potential of the Rockall Trough, Ne Atlantic Margin. *Basin Research*, **17,** 171-201.
722 https://doi.org/10.1111/j.1365-2117.2005.00260.x.
723 Azerêdo, A.C., Duarte, L.V., Henriques, M.H. & Manupella, G. (2003) *Da Dinâmica*
724 *Continental No Triásico Aos Mares Do Jurássico Inferior E Médio*. Instituto Geológico e
725 Mineiro, Lisboa, Portugal. 43
726 Barrier, A., Bischoff, A., Nicol, A., Browne, G.H. & Bassett, K.N. (2021) Relationships between
727 Volcanism and Plate Tectonics: A Case-Study from the Canterbury Basin, New Zealand.
728 *Marine Geology*, **433,** 106397. https://doi.org/10.1016/j.margeo.2020.106397.
729 Bartetzko, A., Delius, H. & Pechnig, R. (2005) Effect of Compositional and Structural
730 Variations on Log Responses of Igneous and Metamorphic Rocks. I: Mafic Rocks.
731 *Geological Society, London, Special Publications*, **240,** 255-278.
732 10.1144/gsl.Sp.2005.240.01.19.
733 Beicip-Franlab (1996) Geochemical Evaluation of the Lusitanian and Porto Basins, BEICIP-
734 FRANLAB**,** 18.
735 Bernard-Griffiths, J., Gruau, G., Cornen, G., Azambre, B. & Mace, J. (1997) Continental
736 Lithospheric Contribution to Alkaline Magmatism: Isotopic (Nd, Sr, Pb) and Geochemical
737 (Ree) Evidence from Serra De Monchique and Mount Ormonde Complexes. *Journal of*
738 *Petrology*, **38,** 115-132. 10.1093/petroj/38.1.115.
739 Bischoff, A., Nicol, A., Cole, J. & Gravley, D. (2019) Stratigraphy of Architectural Elements of
740 a Buried Monogenetic Volcanic System. *Open Geosciences*, **11,** 581.
741 https://doi.org/10.1515/geo-2019-0048.
742 Bischoff, A., Barrier, A., Beggs, M., Nicol, A., Cole, J. & Sahoo, T. (2020) Volcanoes Buried in
743 Te Riu-a-Maui/Zelandia Sedimentary Basins. *New Zealand Journal of Geology and*
744 *Geophysics*, **63,** 378-401. 10.1080/00288306.2020.1773510.
745 Bischoff, A.P., Nicol, A. & Beggs, M. (2017) Stratigraphy of Architectural Elements in a Buried
746 Volcanic System and Implications for Hydrocarbon Exploration. *Interpretation*, **5,** SK141-
747 SK159. 10.1190/int-2016-0201.1.
748 Bronner, A., Sauter, D., Manatschal, G., Péron-Pinvidic, G. & Munschy, M. (2011) Magmatic
749 Breakup as an Explanation for Magnetic Anomalies at Magma-Poor Rifted Margins. *Nature*
750 *Geoscience*, **4,** 549–553. 10.1038/NGEO1201.
751 Callegaro, S., Rapaille, C., Marzoli, A., Bertrand, H., Chiaradia, M., Reisberg, L., Bellieni, G.,
752 Martins, L., Madeira, J., Mata, J., Youbi, N., De Min, A., Azevedo, M.R. & Bensalah, M.K.
753 (2014) Enriched Mantle Source for the Central Atlantic Magmatic Province: New
754 Supporting Evidence from Southwestern Europe. *Lithos*, **188,** 15-32.
755 http://dx.doi.org/10.1016/j.lithos.2013.10.021.
756 Chadwick Jr., W.W., Clague, D.A., Embley, R.W., Perfit, M.R., Butterfield, D.A., Caress, D.W.,
757 Paduan, J.B., Martin, J.F., Sasnett, P., Merle, S.G. & Bobbitt, A.M. (2013) The 1998
758 Eruption of Axial Seamount: New Insights on Submarine Lava Flow Emplacement from
759 High-Resolution Mapping. *Geochemistry, Geophysics, Geosystems*, **14,** 3939-3968.
760 https://doi.org/10.1002/ggge.20202.
761 Civiero, C., Custódio, S., Neres, M., Schlaphorst, D., Mata, J. & Silveira, G. (2021) The Role
762 of the Seismically Slow Central-East Atlantic Anomaly in the Genesis of the Canary and
763 Madeira Volcanic Provinces. *Geophysical Research Letters*, **48,** e2021GL092874.
764 10.1029/2021gl092874.
765 Davison, I. & Barreto, P. (2021) Deformation and Sedimentation Processes, and Hydrocarbon
766 Accumulations on Upturned Salt Diapir Flanks in the Lusitanian Basin, Portugal. *Petroleum*
767 *Geoscience*, **27,** petgeo2019-2138. 10.1144/petgeo2019-138.
768 Escada, C. (2019) Post-Rift Magmatism on the Central West Iberian Margin (Estremadura
769 Spur): New Evidences from Potential Field Data, Universidade de Lisboa.
770 Escada, C., Santos, F., Represas, P., Pereira, R., Mata, J., Rosas, F. & Silva, B. (2019). *Post-*
771 *Rift Magmatism on the Central West Iberian Margin: New Evidence from Magnetic and*
772 *Gravimetric Data Inversion in the Estremadura Spur*. EGU General Assembly 2019,
773 Vienna, Austria, Geophysical Research Abstracts.

774 Ferreira, E. (2017) Caracterização De Fluidos Hidrotermais E Suas Fontes Em Bacias
775 Sedimentares Com Potencial Petrolífero: Aplicação Inovadora De Análises Isotópicas Na
776 Exploração De Petróleo E Gás, Universidade de São Paulo.
777 Franke, D. (2013) Rifting, Lithosphere Breakup and Volcanism: Comparison of Magma-Poor
778 and Volcanic Rifted Margins. *Marine and Petroleum Geology*, **43,** 63-87.
779 Geoffroy, L. (2005) Volcanic Passive Margins. *Comptes Rendus Geoscience*, **337,** 1395-
780 1408. 10.1016/j.crte.2005.10.006.
781 Gpep (1986) The Petroleum Potential of Portugal, Gabinete para a Pesquisa e Exploração de
782 Petróleo. Lisboa**,** 62.
783 Grange, M., Schärer, U., Cornen, G. & Girardeau, J. (2008) First Alkaline Magmatism During
784 Iberia–Newfoundland Rifting. *Terra Nova*, **20,** 494-503. 10.1111/j.1365-
785 3121.2008.00847.x.
786 Grange, M., Scharer, U., Merle, R., Girardeau, J. & Cornen, G. (2010) Plume–Lithosphere
787 Interaction During Migration of Cretaceous Alkaline Magmatism in Sw Portugal: Evidence
788 from U–Pb Ages and Pb–Sr–Hf Isotopes. *Journal of Petrology*, **51,** 1143-1170.
789 10.1093/petrology/egq018.
790 Grosse, P., De Vries, B.V., Euillades, P.A., Kervyn, M. & Petrinovic, I.A. (2012) Systematic
791 Morphometric Characterization of Volcanic Edifices Using Digital Elevation Models.
792 *Geomorphology*, **136,** 114-131. 10.1016/j.geomorph.2011.06.001.
793 Grosse, P., Euillades, P.A., Euillades, L.D. & Van Wyk De Vries, B. (2013) A Global Database
794 of Composite Volcano Morphometry. *Bulletin of Volcanology*, **76,** 1-16. 10.1007/s00445-
795 013-0784-4.
796 Hubbard, R.J., Pape, J. & Roberts, D.G. (1985) Depositional Sequence Stratigraphy Mapping
797 to Illustrate the Evolution of a Passive Continental Margin. In: *Seismic Stratigraphy Ii: An*
798 *Integrated Approach* (Ed. by O. R. Berg & D. Woolverton), **39**, 93-115. AAPG, Tulsa,
799 Oklahoma.
800 Huismans, R.S., Podladchikov, Y.Y. & Cloetingh, S. (2001) Transition from Passive to Active
801 Rifting: Relative Importance of Asthenospheric Doming and Passive Extension of the
802 Lithosphere. *Journal of Geophysical Research: Solid Earth*, **106,** 11271-11291.
803 10.1029/2000jb900424.
804 Jackson, C., Magee, C. & Jacquemyn, C. (2020) Rift-Related Magmatism Influences
805 Petroleum System Development in the Ne Irish Rockall Basin, Offshore Ireland. *Petroleum*
806 *Geoscience*, **26,** 511-524. 10.1144/petgeo2018-020.
807 Jackson, C.a.L., Schofield, N. & Golenkov, B. (2013) Geometry and Controls on the
808 Development of Igneous Sill-Related Forced Folds: A 2-D Seismic Reflection Case Study
809 from Offshore Southern Australia. *Geological Society of America Bulletin*, **125,** 1874-1890.
810 10.1130/b30833.1.
811 Kereszturi, Á., Hargitai, H. & Zimbelman, J. (2015) Lava Flow. In: *Encyclopedia of Planetary*
812 *Landforms* (Ed. by H. Hargitai & Á. Kereszturi). Springer, New York, U.S.A.
813 Kullberg, J.C. & Kullberg, M.C. (2017) The Tectono-Stratigraphic Evolution of an Atlantic-Type
814 Basin: An Example from the Arrábida Sector of the Lusitanian Basin. *Ciências da Terra -*
815 *Earth Sciences Journal*, **19,** 55-74. 10.21695/cterra/esj.v19i1.354.
816 Leroy, M., Gueydan, F. & Dauteuil, O. (2008) Uplift and Strength Evolution of Passive Margins
817 Inferred from 2-D Conductive Modelling. *Geophysical Journal International*, **172,** 464-476.
818 10.1111/j.1365-246X.2007.03566.x.
819 Magee, C., Hunt-Stewart, E. & Jackson, C.a.L. (2013) Volcano Growth Mechanisms and the
820 Role of Sub-Volcanic Intrusions: Insights from 2d Seismic Reflection Data. *Earth and*
821 *Planetary Science Letters*, **373,** 41-53. https://doi.org/10.1016/j.epsl.2013.04.041.
822 Magee, C., Maharaj, S.M., Wrona, T. & Jackson, C.a.L. (2015) Controls on the Expression of
823 Igneous Intrusions in Seismic Reflection Data. *Geosphere*, **11,** 1024-1041.
824 10.1130/ges01150.1.
825 Magee, C., Jackson, C.a.-L., Hardman, J.P. & Reeve, M.T. (2017) Decoding Sill Emplacement
826 and Forced Fold Growth in the Exmouth Sub-Basin, Offshore Northwest Australia:
827 Implications for Hydrocarbon Exploration. *Interpretation*, **5,** SK11-SK22. 10.1190/int-2016-
828 0133.1.

Manatschal, G. (2004) New Models for Evolution of Magma-Poor Rifted Margins Based on a Review of Data and Concepts from West Iberia and the Alps. *International Journal of Earth Sciences*, **93,** 432-466. 10.1007/s00531-004-0394-7.

Manupella, G., Ferreira, A.B., Diniz, J., Callapez, P., Ribeiro, M.L., Pais, J., Rebêlo, L., Cabral, J., Moniz, C., Baptista, R., Henriques, P., Falé, P., Lourenço, C., Sampaio, J., Midões, C. & Zbyszewski, G. (2011) *Notícia Explicativa Da Carta Geológica 34-B, Loures, 1:50.000*. Laboratório Nacional de Energia e Geologia, Lisboa. 57

Mark, N.J., Schofield, N., Pugliese, S., Watson, D., Holford, S., Muirhead, D., Brown, R. & Healy, D. (2018) Igneous Intrusions in the Faroe Shetland Basin and Their Implications for Hydrocarbon Exploration; New Insights from Well and Seismic Data. *Marine and Petroleum Geology*, **92,** 733-753. https://doi.org/10.1016/j.marpetgeo.2017.12.005.

Marques, F.O., Azerêdo, A.C., Cabral, M.C. & Santos, V. (1998). *Preliminary Study of a Proposed New Cartographic Unit in the Lisbon Region: The Fanhões Conglomerates*. V Congresso Nacional de Geologia, Lisbon, Instituto Geológico e Mineiro.

Martín-Chivelet, J., Floquet, M., García-Senz, J., Callapez, P.M., López-Mir, B., Muñoz, J.A., Barroso-Barcenilla, F., Segura, M., Soares, A.F., Dinis, P.M., Marques, J.F. & Arbués, P. (2019) Late Cretaceous Post-Rift to Convergence in Iberia. In: *The Geology of Iberia: A Geodynamic Approach* (Ed. by, *Regional Geology Reviews*, **3**, 285-376. Springer.

Martins, L.T., Madeira, J., Youbi, N., Munhá, J., Mata, J. & Kerrich, R. (2008) Rift-Related Magmatism of the Central Atlantic Magmatic Province in Algarve, Southern Portugal. *Lithos*, **101,** 102–124.

Mata, J., Alves, C.F., Martins, L., Miranda, R., Madeira, J., Pimentel, N., Martins, S., Azevedo, M.R., Youbi, N., De Min, A., Almeida, I.M., Bensalah, M.K. & Terrinha, P. (2015) $^{40}ar/^{39}ar$ Ages and Petrogenesis of the West Iberian Margin Onshore Magmatism at the Jurassic-Cretaceous Transition: Geodynamic Implications and Assessment of Open-System Processes Involving Saline Materials. *Lithos*, **236-237,** 156-172. http://dx.doi.org/10.1016/j.lithos.2015.09.001.

Mata, J., Martins, S., Mattielli, N., Madeira, J., Faria, B., Ramalho, R.S., Silva, P., Moreira, M., Caldeira, R., Moreira, M., Rodrigues, J. & Martins, L. (2017) The 2014–15 Eruption and the Short-Term Geochemical Evolution of the Fogo Volcano (Cape Verde): Evidence for Small-Scale Mantle Heterogeneity. *Lithos*, **288-289,** 91-107. https://doi.org/10.1016/j.lithos.2017.07.001.

Matton, G. & Jébrak, M. (2009) The Cretaceous Peri-Atlantic Alkaline Pulse (Paap): Deep Mantle Plume Origin or Shallow Lithospheric Break-Up? *Tectonophysics*, **469,** 1-12. https://doi.org/10.1016/j.tecto.2009.01.001.

Mclean, C.E., Schofield, N., Brown, D.J., Jolley, D.W. & Reid, A. (2017) 3d Seismic Imaging of the Shallow Plumbing System beneath the Ben Nevis Monogenetic Volcanic Field: Faroe–Shetland Basin. *Journal of the Geological Society*, **174,** 468-485. 10.1144/jgs2016-118.

Merle, R., Jourdan, F. & Girardeau, J. (2018) Geochronology of the Tore-Madeira Rise Seamounts and Surrounding Areas: A Review. *Australian Journal of Earth Sciences*, **65,** 591-605. 10.1080/08120099.2018.1471005.

Merle, R.E., Jourdan, F., Chiaradia, M., Olierook, H.K.H. & Manatschal, G. (2019) Origin of Widespread Cretaceous Alkaline Magmatism in the Central Atlantic: A Single Melting Anomaly? *Lithos*, **342-343,** 480-498. https://doi.org/10.1016/j.lithos.2019.06.002.

Miranda, R., Valadares, V., Terrinha, P., Mata, J., Azevedo, M.D.R., Gaspar, M., Kullberg, J.C. & Ribeiro, C. (2009) Age Constrains on the Late Cretaceous Alkaline Magmatism on the West Iberian Margin. *Cretaceous Research*, **30,** 575-586.

Miranda, R. (2010) Petrogenesis and Geochronology of the Late Cretaceous Alkaline Magmatism in the West Iberian Margin, Universidade de Lisboa, Lisboa.

Miranda, R., Terrinha, P., Mata, J., Azevêdo, M.D.R., Chadwick, J., Lourenço, N. & Moreira, M. (2010). *Caracterização Geoquímica Do Monte Submarino De Fontanelas, Margem Oeste Ibérica*. X Congresso de geoquímica dos países de lingua oficial portuguesa, XVI Semana de geoquímica, Porto, Portugal, Universidade do Porto.

Neres, M., Bouchez, J.L., Terrinha, P., Font, E., Moreira, M., Miranda, R., Launeau, P. & Carvallo, C. (2014) Magnetic Fabric in a Cretaceous Sill (Foz Da Fonte, Portugal): Flow Model and Implications for Regional Magmatism. *Geophysical Journal International*, **199,** 78-101. 10.1093/gji/ggu250.

Neres, M., Terrinha, P., Custódio, S., Silva, S.M., Luis, J. & Miranda, J.M. (2018) Geophysical Evidence for a Magmatic Intrusion in the Ocean-Continent Transition of the Sw Iberia Margin. *Tectonophysics*, **744,** 118-133. https://doi.org/10.1016/j.tecto.2018.06.014.

Niyazi, Y., Eruteya, O.E., Warne, M. & Ierodiaconou, D. (2021a) Discovery of Large-Scale Buried Volcanoes within the Cenozoic Succession of the Prawn Platform, Offshore Otway Basin, Southeastern Australia. *Marine and Petroleum Geology*, **123,** 104747. https://doi.org/10.1016/j.marpetgeo.2020.104747.

Niyazi, Y., Warne, M. & Ierodiaconou, D. (2021b) Post-Rift Magmatism and Hydrothermal Activity in the Central Offshore Otway Basin and Implications for Igneous Plumbing Systems. *Marine Geology*, **438,** 106538. https://doi.org/10.1016/j.margeo.2021.106538.

Oyarzun, R., Doblas, M., López-Ruiz, J. & María Cebrá, J. (1997) Opening of the Central Atlantic and Asymmetric Mantle Upwelling Phenomena: Implications for Long-Lived Magmatism in Western North Africa and Europe. *Geology*, **25,** 727-730. 10.1130/0091-7613(1997)025<0727:ootcaa>2.3.co;2.

Pereira, R., Alves, T.M. & Mata, J. (2017) Alternating Crustal Architecture in West Iberia: A Review of Its Significance in the Context of Ne Atlantic Rifting. *Journal of the Geological Society*, **174,** 522-540. 10.1144/jgs2016-050.

Pereira, R. & Barreto, P. (2018). *Evidence and Significance of Buried Magmatic Features Offshore the West Iberian Margin*. AAPG Europe Conference and Exhibition, Lisbon, Portugal.

Pereira, R., Rosas, F., Mata, J., Represas, P., Escada, C. & Silva, B. (2021) Interplay of Tectonics and Magmatism During Post-Rift Inversion on the Central West Iberian Margin (Estremadura Spur). *Basin Research*, **33,** 1497-1519. 10.1111/bre.12524.

Pérez-Gussinyé, M., Morgan, J.P., Reston, T.J. & Ranero, C.R. (2006) The Rift to Drift Transition at Non-Volcanic Margins: Insights from Numerical Modelling. *Earth and Planetary Science Letters*, **244,** 458-473. https://doi.org/10.1016/j.epsl.2006.01.059.

Peterson, D.W. & Tilling, R.I. (1980) Transition of Basaltic Lava from Pahoehoe to Aa, Kilauea Volcano, Hawaii: Field Observations and Key Factors. *Journal of Volcanology and Geothermal Research*, **7,** 271-293. https://doi.org/10.1016/0377-0273(80)90033-5.

Planke, S., Rasmussen, T., Rey, S.S. & Myklebust, R. (2005) Seismic Characteristics and Distribution of Volcanic Intrusions and Hydrothermal Vent Complexes in the Vøring and Møre Basins. *Geological Society, London, Petroleum Geology Conference series*, **6,** 833-844. 10.1144/0060833.

Planke, S., Svensen, H., Myklebust, R., Bannister, S., Manton, B. & Lorenz, L. (2015) Geophysics and Remote Sensing. In: *Physical Geology of Shallow Magmatic Systems* (Ed. by, 131-146.

Planke, S., Millett, J.M., Maharjan, D., Jerram, D.A., Abdelmalak, M.M., Groth, A., Hoffmann, J., Berndt, C. & Myklebust, R. (2017) Igneous Seismic Geomorphology of Buried Lava Fields and Coastal Escarpments on the Vøring Volcanic Rifted Margin. *Interpretation*, **5,** SK161-SK177. 10.1190/int-2016-0164.1.

Pyle, D.M. (2015) Sizes of Volcanic Eruptions, in Sigurdsson, H., Houghton, B., Mcnutt, S., Rymer, H. And Stix, J. Eds., 2000. The Encyclopedia of Volcanoes. Academic Press. In: *The Encyclopedia of Volcanoes* (Ed. by H. Sigurdsson), 257-264. Elsevier.

Ramalho, M.M., Pais, J., Rey, J., Berthou, P.-Y., Alves, C.a.M., Palacios, T., Leal, N. & Kullberg, M.C. (1993) Notícia Explicativa Da Folha 34-a, Sintra, 1:50000. S. G. d. Portugal**,** 77.

Rey, J., Dinis, J.L., Callapez, P. & Cunha, P.P. (2006) *Da Rotura Continental À Margem Passiva: Composição E Evolução Do Cretácico De Portugal*. INETI, Lisboa, Portugal. 75

Reynolds, P., Holford, S., Schofield, N. & Ross, A. (2017a) The Shallow Depth Emplacement of Mafic Intrusions on a Magma-Poor Rifted Margin: An Example from the Bight Basin,

Southern Australia. *Marine and Petroleum Geology*, **88,** 605-616. https://doi.org/10.1016/j.marpetgeo.2017.09.008.
Reynolds, P., Holford, S., Schofield, N. & Ross, A. (2017b) Three-Dimensional Seismic Imaging of Ancient Submarine Lava Flows: An Example from the Southern Australian Margin. *Geochemistry, Geophysics, Geosystems*, **18,** 3840-3853. https://doi.org/10.1002/2017GC007178.
Rock, N.M.S. (1982) The Late Cretaceous Alkaline Igneous Province in the Iberian Peninsula, and Its Tectonic Significance. *Lithos*, **15,** 111-131. https://doi.org/10.1016/0024-4937(82)90004-4.
Schofield, N.J., Brown, D.J., Magee, C. & Stevenson, C.T. (2012) Sill Morphology and Comparison of Brittle and Non-Brittle Emplacement Mechanisms. *Journal of the Geological Society*, **169,** 127-141. 10.1144/0016-76492011-078.
Senger, K., Millett, J., Planke, S., Ogata, K., Haug Eide, C., Festøy, M., Galland, O. & Jerram, D.A. (2017) Effects of Igneous Intrusions on the Petroleum System: A Review. *First Break*, **35**. https://doi.org/10.3997/1365-2397.2017011.
Sheridan, M.F. & Wohletz, K.H. (1981) Hydrovolcanic Explosions: The Systematics of Water-Pyroclast Equilibration. *Science*, **212,** 1387-1389. doi:10.1126/science.212.4501.1387.
Silva, E.A., Miranda, J.M., Luis, J.F. & Galdeano, A. (2000) Correlation between the Palaeozoic Structures from West Iberian and Grand Banks Margins Using Inversion of Magnetic Anomalies. *Tectonophysics*, **321,** 57-71. https://doi.org/10.1016/S0040-1951(00)00080-9.
Silva, S.D. & Lindsay, J.M. (2015) Primary Volcanic Landforms. In: *The Encyclopedia of Volcanoes* (Ed. by H. Sigurdsson), 273-297.
Simões, P., Neres, M. & Terrinha, P. (2020). *Joint Modeling of Seismic, Magnetic and Gravimetric Data Unravels the Extent of the Late Cretaceous Magmatic Province on the Estremadura Spur Offshore West Iberia*. EGU General Assembly.
Smallwood, J.R. & Maresh, J. (2002) The Properties, Morphology and Distribution of Igneous Sills: Modelling, Borehole Data and 3d Seismic from the Faroe-Shetland Area. *Geological Society, London, Special Publications*, **197,** 271-306. 10.1144/gsl.Sp.2002.197.01.11.
Sohn, Y.K. (1996) Hydrovolcanic Processes Forming Basaltic Tuff Rings and Cones on Cheju Island, Korea. *GSA Bulletin*, **108,** 1199-1211.
Sparks, R.S.J. & Wadge, G. (1975) Geological and Geochemical Studies of the Sintra Alkaline Igneous Complex, Portugal. *Bulletin Volcanologique*, **39,** 385-406. 10.1007/BF02597263.
Sun, Q., Jackson, C.a.L., Magee, C., Mitchell, S.J. & Xie, X. (2019) Extrusion Dynamics of Deepwater Volcanoes Revealed by 3-D Seismic Data. *Solid Earth*, **10,** 1269-1282. 10.5194/se-10-1269-2019.
Sun, Q., Magee, C., Jackson, C.a.L., Mitchell, S.J. & Xie, X. (2020) How Do Deep-Water Volcanoes Grow? *Earth and Planetary Science Letters*, **542**. 10.1016/j.epsl.2020.116320.
Terrinha, P., Pueyo, E.L., Aranguren, A., Kullberg, J.C., Kullberg, M.C., Casas-Sainz, A. & Azevedo, M.D.R. (2017) Gravimetric and Magnetic Fabric Study of the Sintra Igneous Complex: Laccolith-Plug Emplacement in the Western Iberian Passive Margin. *International Journal of Earth Sciences*, **107,** 1807-1833. 10.1007/s00531-017-1573-7.
Thomson, K. (2004) Volcanic Features of the North Rockall Trough: Application of Visualisation Techniques on 3d Seismic Reflection Data. *Bulletin of Volcanology*, **67,** 116-128. 10.1007/s00445-004-0363-9.
Thomson, K. & Hutton, D. (2004) Geometry and Growth of Sill Complexes: Insights Using 3d Seismic from the North Rockall Trough. *Bulletin of Volcanology*, **66,** 364-375. 10.1007/s00445-003-0320-z.
Verati, C., Rapaille, C., Feraud, G., Marzoli, A., Bertrand, H. & Youbi, N. (2007) Ar-40/Ar-39 Ages and Duration of the Central Atlantic Magmatic Province Volcanism in Morocco and Portugal and Its Relation to the Triassic-Jurassic Boundary. *Palaeogeography, Palaeoclimatology, Palaeoecology*, **244,** 308-325.
Verwoerd, W.J. & Chevallier, L. (1987) Contrasting Types of Surtseyan Tuff Cones on Marion and Prince Edward Islands, Southwest Indian Ocean. *Bulletin of Volcanology*, **49,** 399-413. 10.1007/BF01046633.

992 Walker, F., Schofield, N., Millett, J., Jolley, D., Holford, S., Planke, S., Jerram, D.A. &
993 Myklebust, R. (2020) Inside the Volcano: Three-Dimensional Magmatic Architecture of a
994 Buried Shield Volcano. *Geology*. 10.1130/g47941.1.
995 White, J.D.L., Mcphie, J. & Soule, S.A. (2015) Chapter 19 - Submarine Lavas and
996 Hyaloclastite. In: *The Encyclopedia of Volcanoes (Second Edition)* (Ed. by H. Sigurdsson),
997 363-375. Academic Press, Amsterdam.
998 Witt, W.G. (1977) Stratigraphy of the Lusitanian Basin, Shell Prospex Portuguesa**,** 61.
999 Wright, J.B. (1969) Re-Interpretation of a Mixed Petrographic Province—the Sintra Intrusive
1000 Complex (Portugal) and Related Rocks. *Geologische Rundschau*, **58,** 538-564.
1001 Zhao, F., Alves, T.M., Wu, S., Li, W., Huuse, M., Mi, L., Sun, Q. & Ma, B. (2016) Prolonged
1002 Post-Rift Magmatism on Highly Extended Crust of Divergent Continental Margins (Baiyun
1003 Sag, South China Sea). *Earth and Planetary Science Letters*, **445,** 79-91.
1004 https://doi.org/10.1016/j.epsl.2016.04.001.

1005

1006

Figures

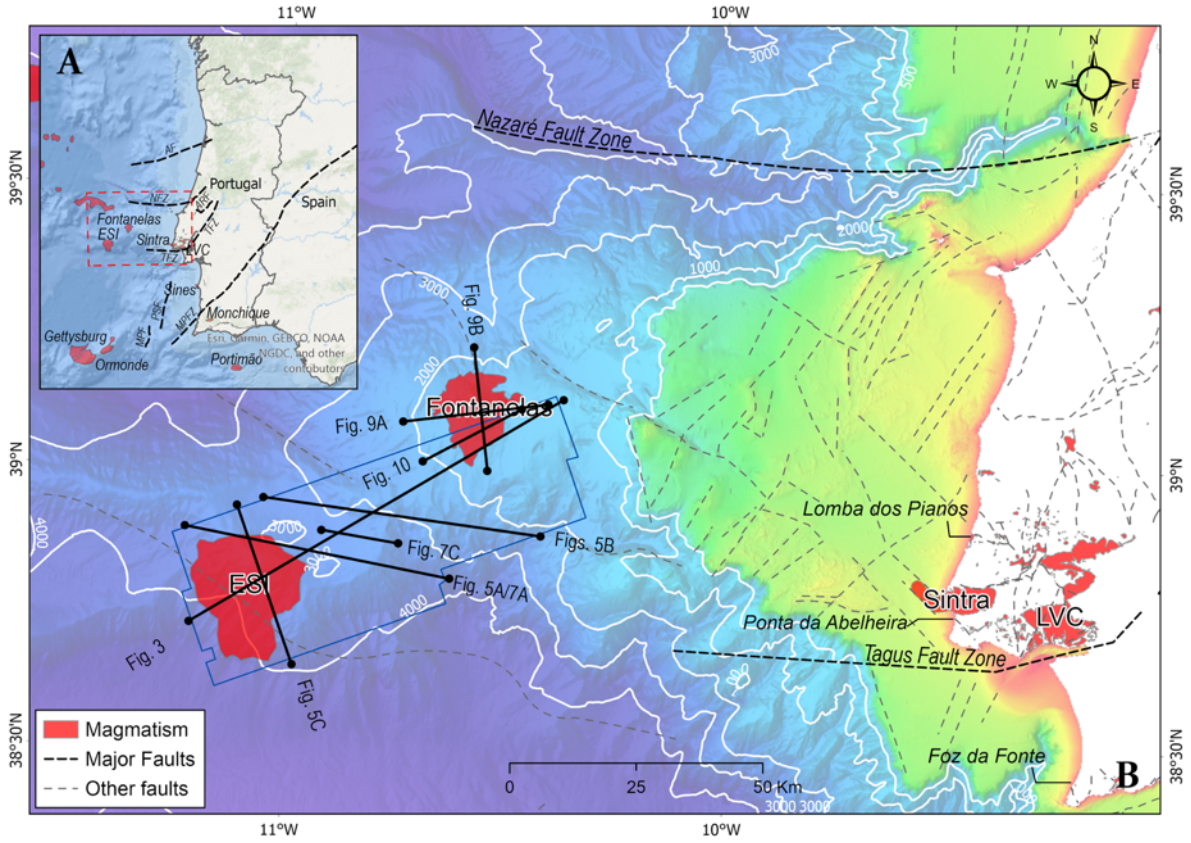

Figure 1. Location of the area of interest showing the distribution of magmatism on the central West Iberian Margin. ESI – Estremadura Spur Intrusion, LVC – Lisbon Volcanic Complex, AF – Aveiro Fault, NFZ – Nazaré Fault Zone, TFZ – Tagus Fault Zone, PSF – Pereira de Sousa Fault, MPF – Marquês de Pombal Fault, MPFZ – Messejana-Plasencia Fault Zone.

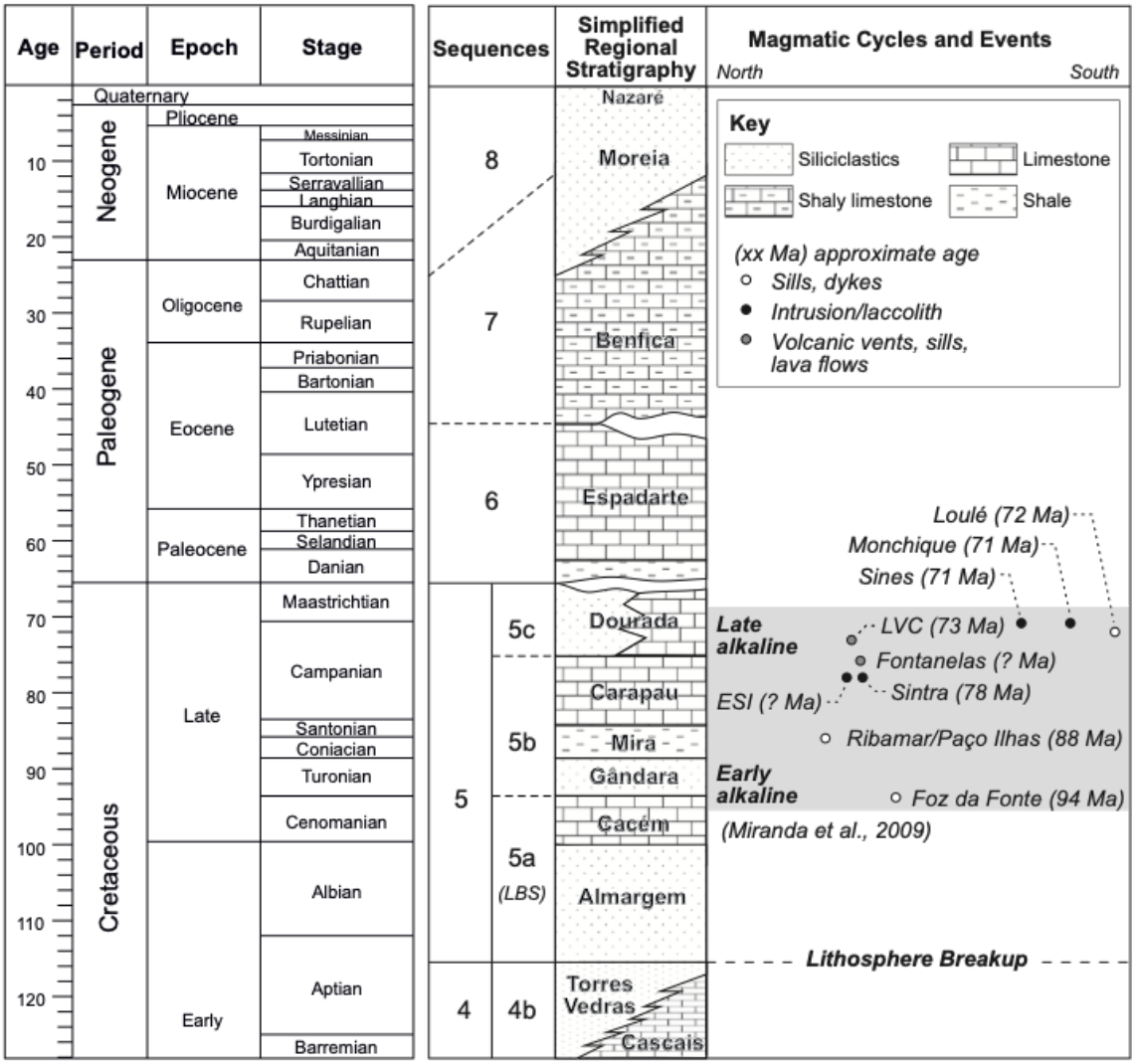

Figure 2. Stratigraphic framework of the West Iberian Margin showing the distinct megasequences, lithostratigraphic units and evidence of the Late Cretaceous alkaline magmatism. LBS – Lithosphere Breakup Sequence (Unit 5a).

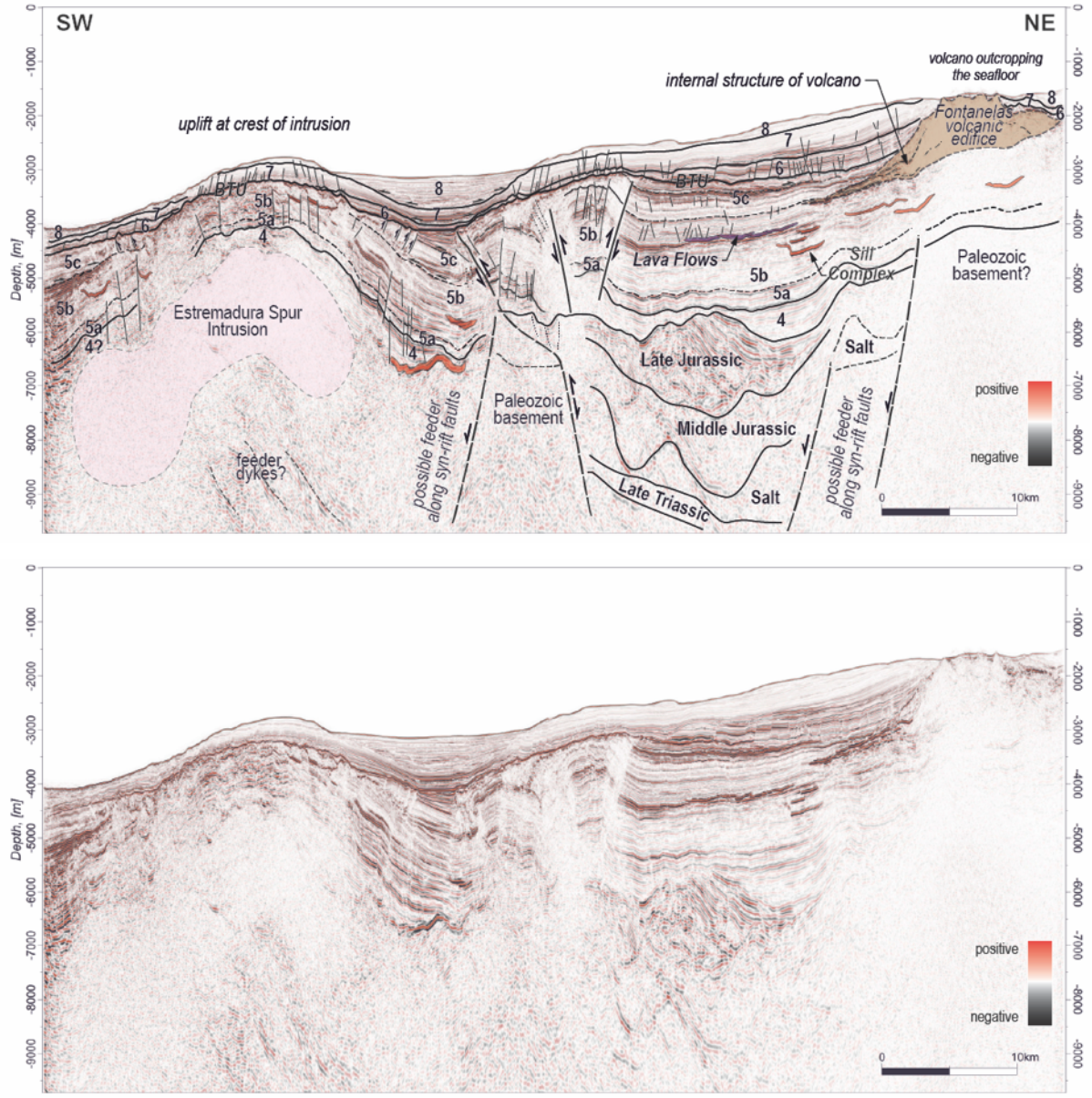

Figure 3. Seismic line (in depth) across the Estremadura Spur, showing the evidence of the Fontanelas volcano, the Estremadura Spur Intrusion with associated sills (red) and lava flows (purple), as part of the larger magmatic plumbing system of the Late Cretaceous. BTU – Base Tertiary Unconformity.

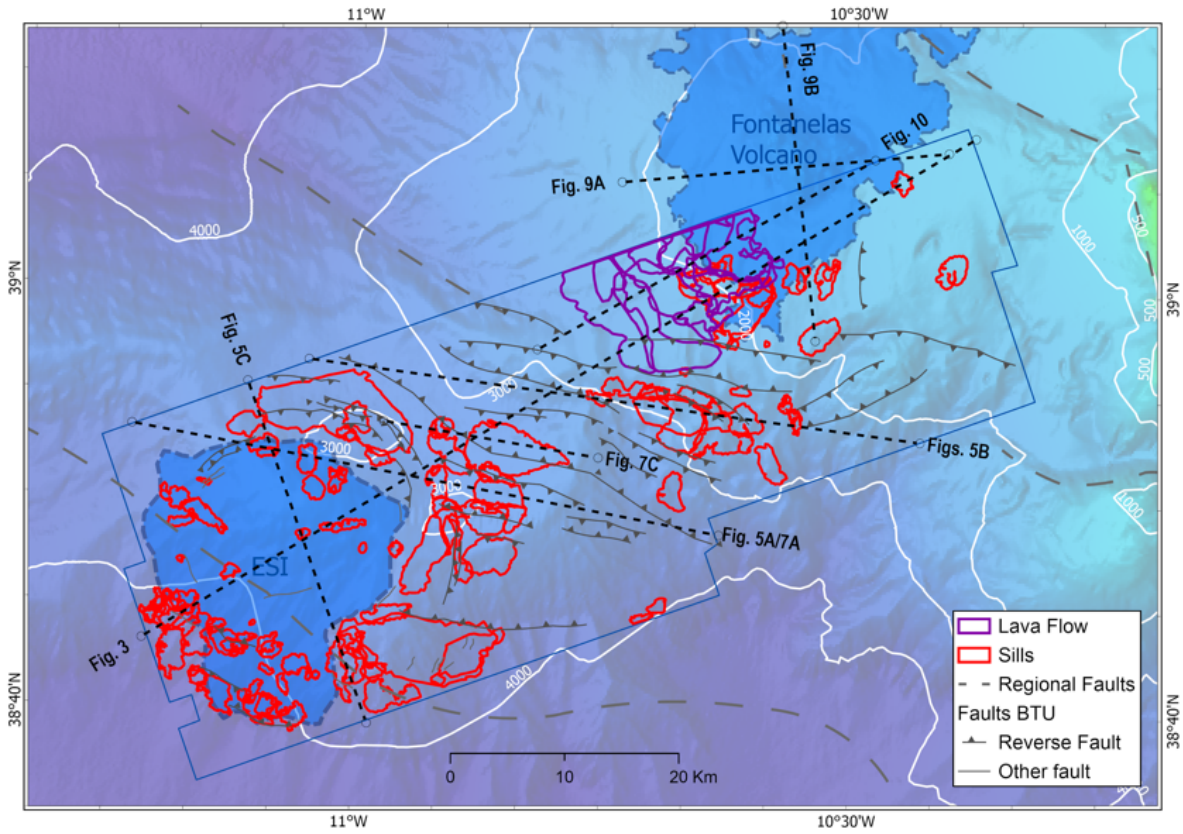

Figure 4. Map showing the location of the Estremadura Spur Intrusion (ESI), the Fontanelas volcano and the dominant distribution of sills (red) and lava flows (purple).

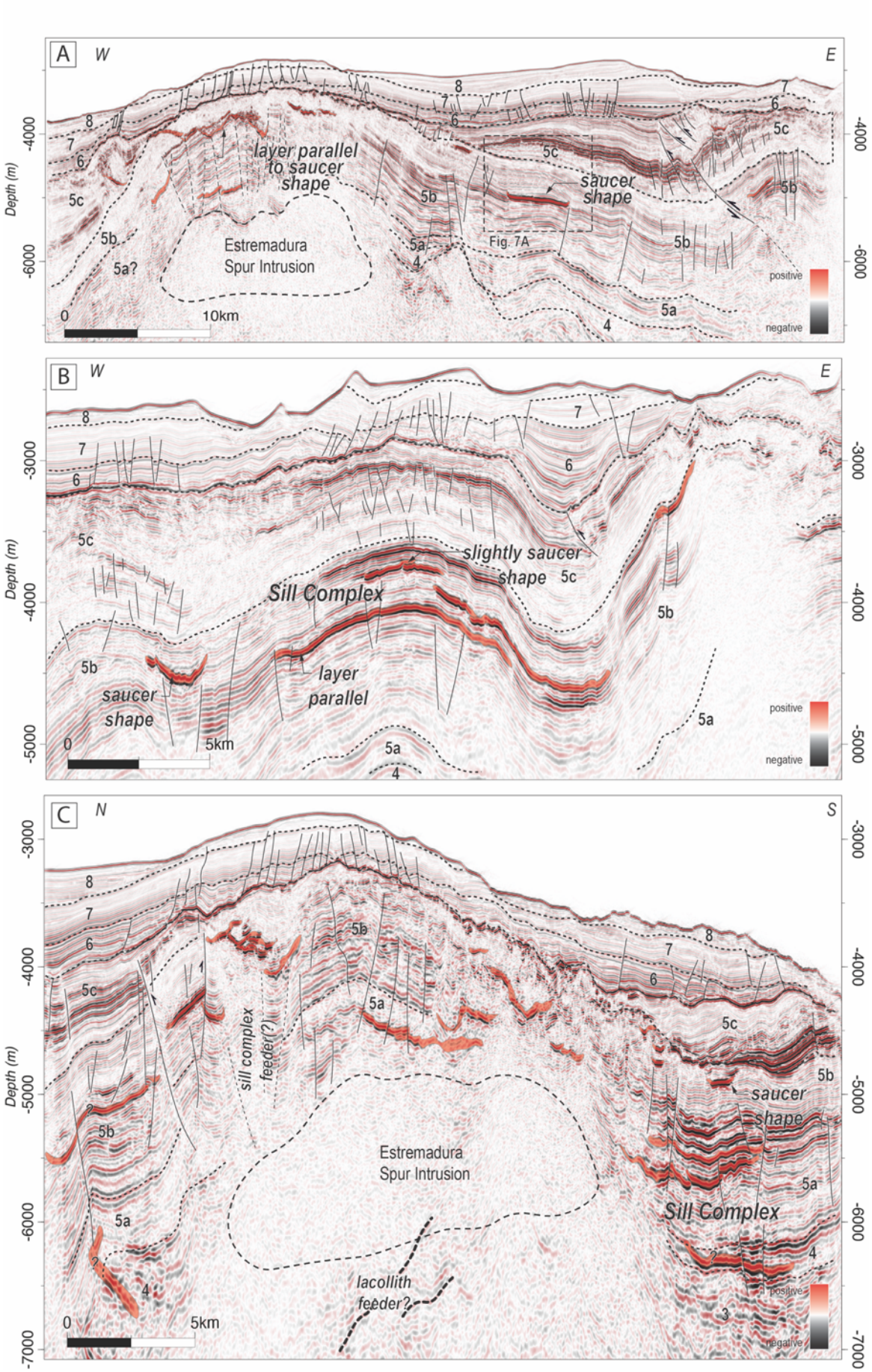
A
W
E
layer parallel to saucer shape
saucer shape
Estremadura Spur Intrusion
Fig. 7A
5c
5b
5a?
5a
4
positive
negative
0
10km
Depth (m)
-4000
-6000
B
W
E
slightly saucer shape
Sill Complex
layer parallel
saucer shape
5km
-3000
-4000
-5000
C
N
S
sill complex feeder(?)
Estremadura Spur Intrusion
Sill Complex
saucer shape
laccolith feeder?
5km
-3000
-4000
-5000
-6000
-7000

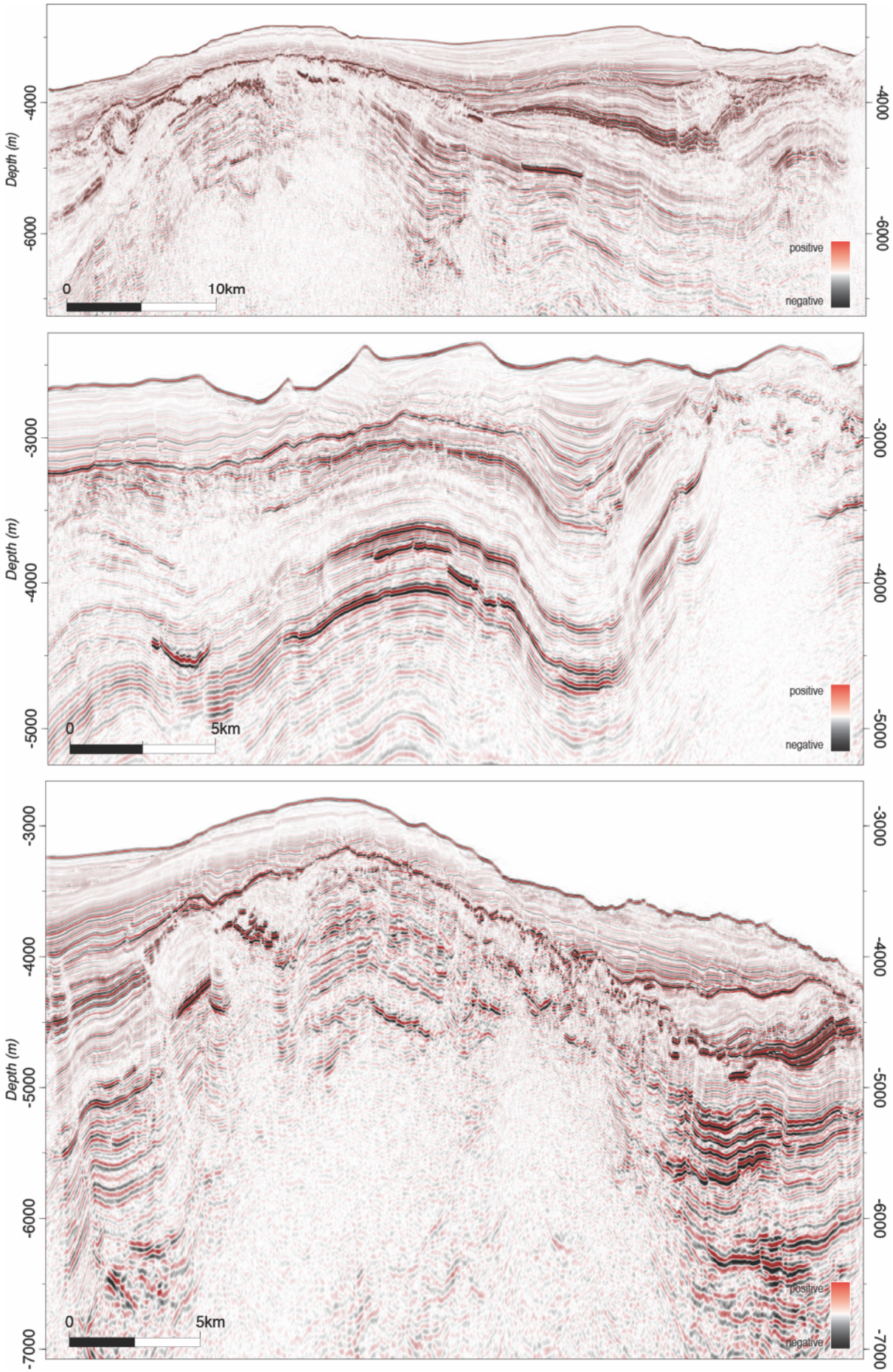
Depth (m)
-4000
-6000
0
10km
positive
negative
Depth (m)
-3000
-4000
-5000
0
5km
positive
negative
Depth (m)
-3000
-4000
-5000
-6000
-7000
0
5km
positive
negative

Figure 5. Seismic lines (in depth) showing the distribution and different geometry of sills (in red) throughout the Estremadura Spur. Note that sills and sill complexes are dominantly emplaced within sequence 5b. Location of seismic lines in figure 4.

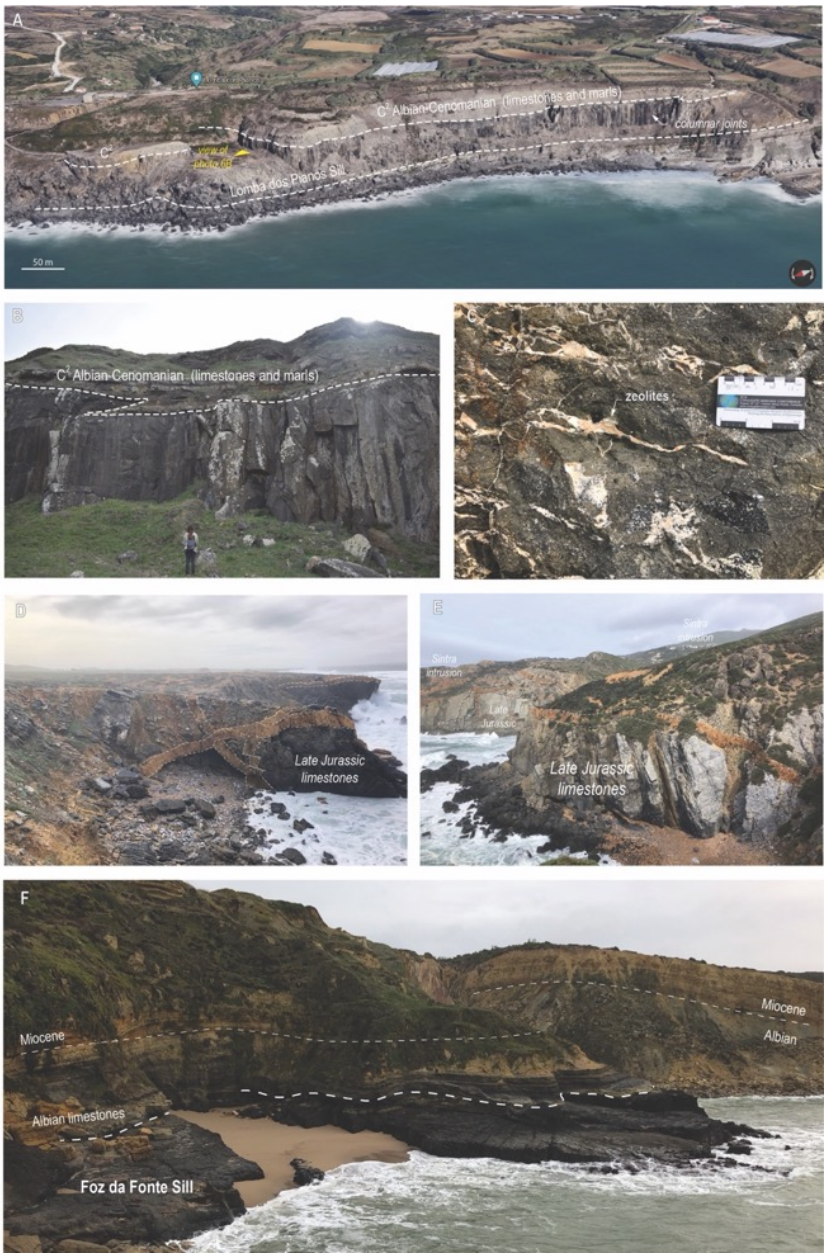

Figure 6. Outcropping examples of the Late Cretaceous magmatism. A) Lomba dos Pianos sill, as seen on Google Maps perspective, showing the relation between the Albian-Cenomanian limestones and marls. Approximate thickness of the sill is 30-40 m. Lat: 38°53'36.22"N, Long: 9°26'18.00"W. B) Detail of the Lomba dos Pianos sill showing the top contact with limestones, evidencing prismatic joints. View to the South. C) Detail of the basaltic sill, showing zeolites filling fractures. D) Crosscutting trachytic-basaltic(?) ring dykes associated with the Sintra intrusion, at Ponta da Abelheira. View to the South. Lat: 38°44'52.81"N; Long: 9°28'18.36"W. E) Trachytic-basaltic(?) dykes and sills crosscutting late Jurassic limestones at Ponta da Abelheira, showing the landscape of the Sintra massif at a distance. F) The Foz da Fonte sill intruding Albian limestones, an example of forced folding associated with shallow magma emplacement; Lat: 38°27'3.91"N, Long: 9°12'6.25"W.

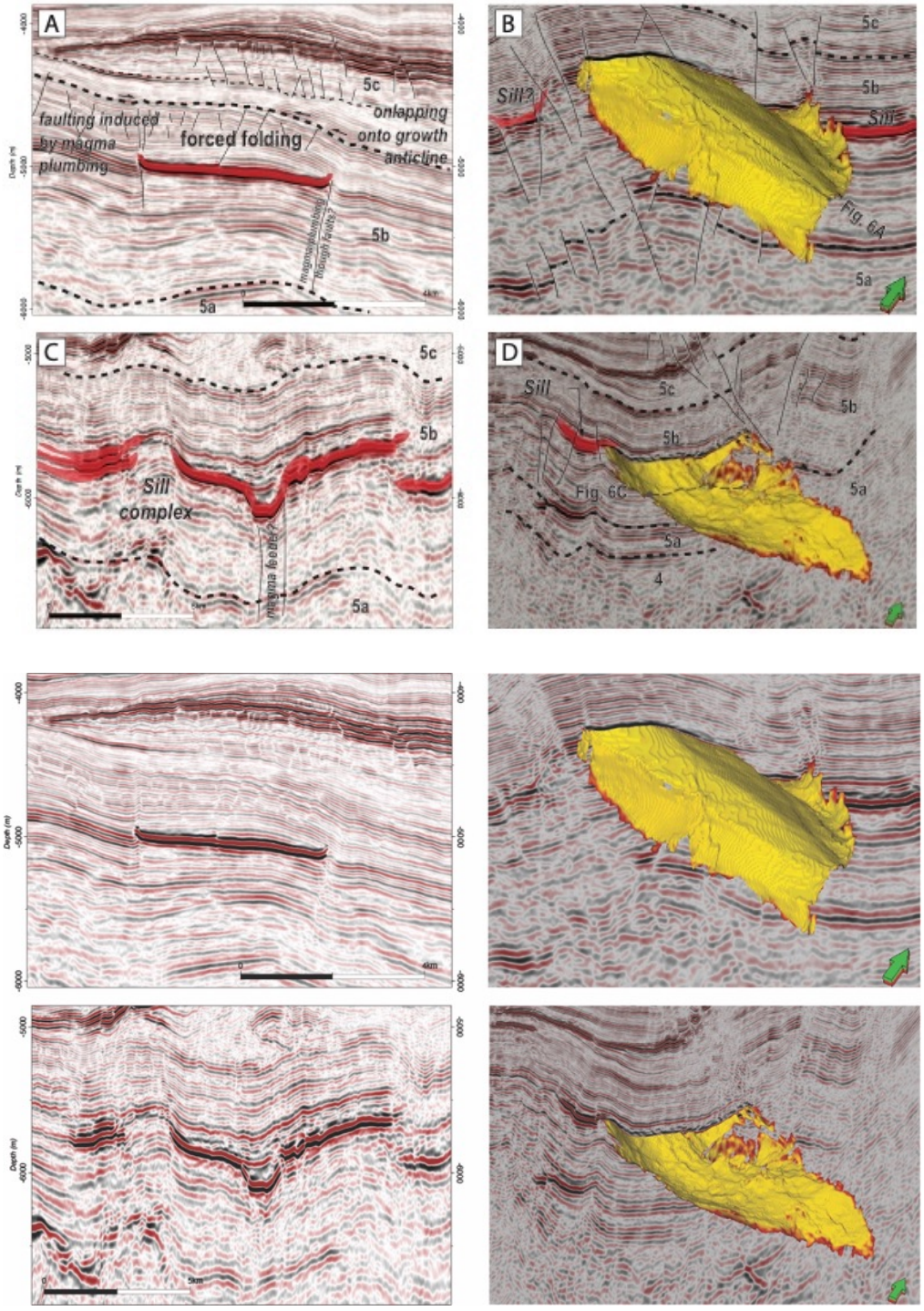

Figure 7. Details of sills intruding the Estremadura Spur. A) Seismic section showing an example of a planar-slightly saucer chape sill intruding unit 5b, with forced folding and faulting of overburden strata, with onlaps at base of sequence 5c. Note faulting at the edge of sill, tentatively interpreted as conduit for magma emplacement. B) 3D view of the sill showing the flanks of the sill. C) Sill complex intruding unit 5b, highlighting the presence of a saucer-shape sill and possible magma conduit. D) 3D view of the sill, showing it complex geometry and possible source of magma flow.

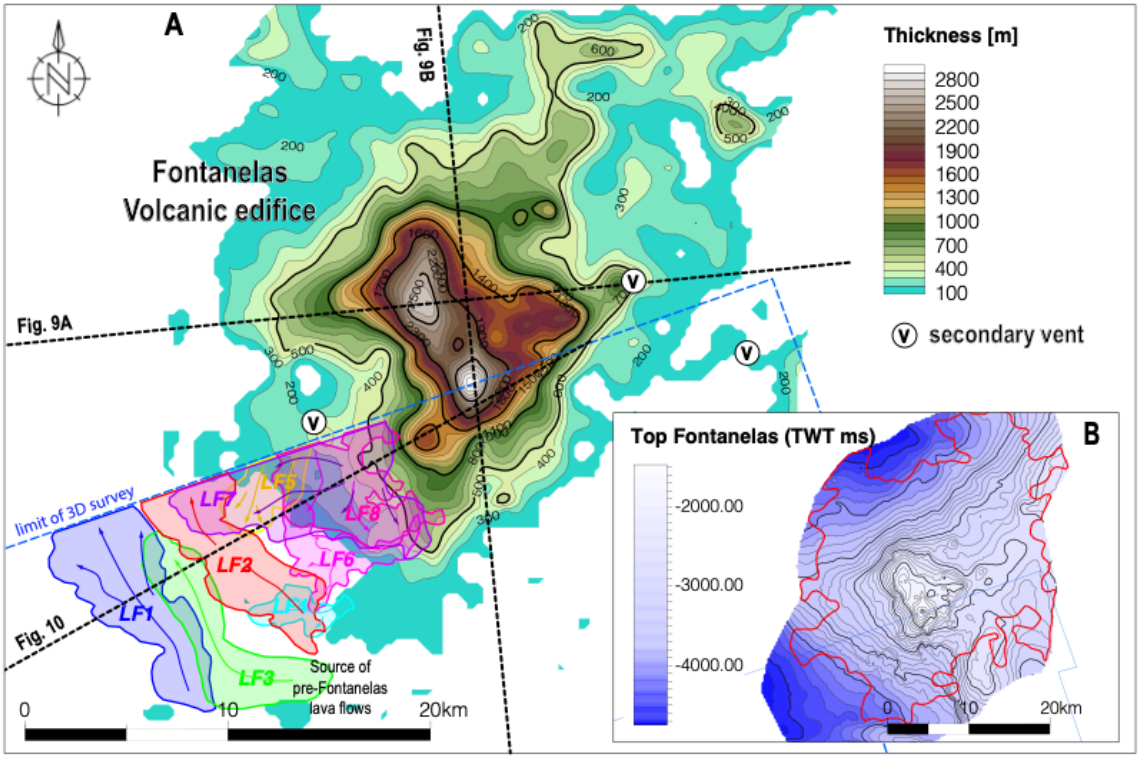

Figure 8. A) Thickness map of the Fontanelas volcanic edifice, based on 2D/3D seismic data, with associated lavas (1 to 8), with interpreted flow directions from a common source. Note the presence of secondary volcanic vents. B) TWT structural map of the Fontanelas volcano.

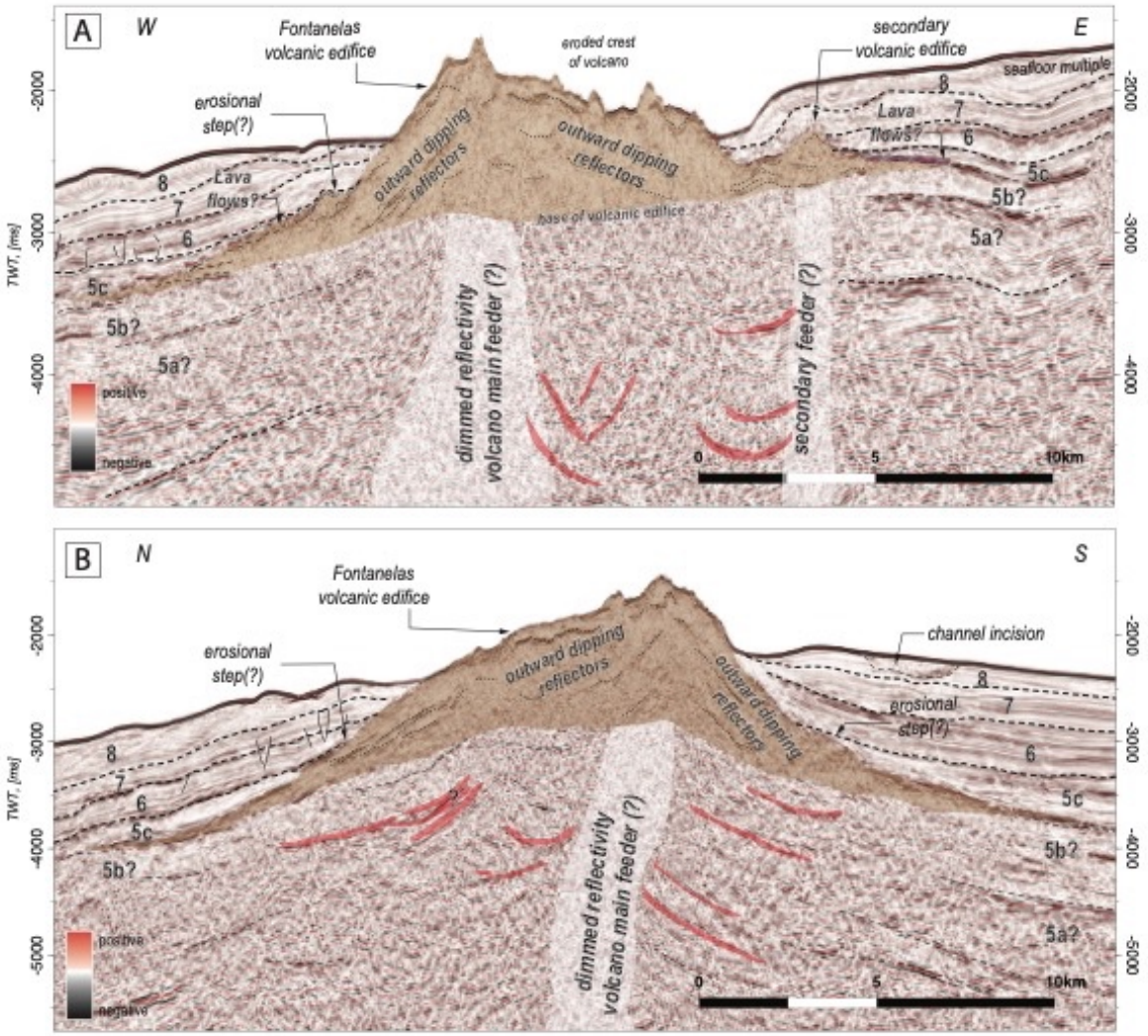
A
W
E
Fontanelas volcanic edifice
eroded crest of volcano
secondary volcanic edifice
seafloor multiple
erosional step(?)
outward dipping reflectors
outward dipping reflectors
Lava flows?
base of volcanic edifice
8
7
6
5c
5b?
5a?
dimmed reflectivity volcano main feeder (?)
secondary feeder (?)
positive
negative
0
5
10km
TWT, [ms]
-2000
-3000
-4000
B
N
S
Fontanelas volcanic edifice
channel incision
erosional step(?)
outward dipping reflectors
outward dipping reflectors
erosional step(?)
8
7
6
5c
5b?
5a?
dimmed reflectivity volcano main feeder (?)
positive
negative
0
5
10km
TWT, [ms]
-2000
-3000
-4000
-5000

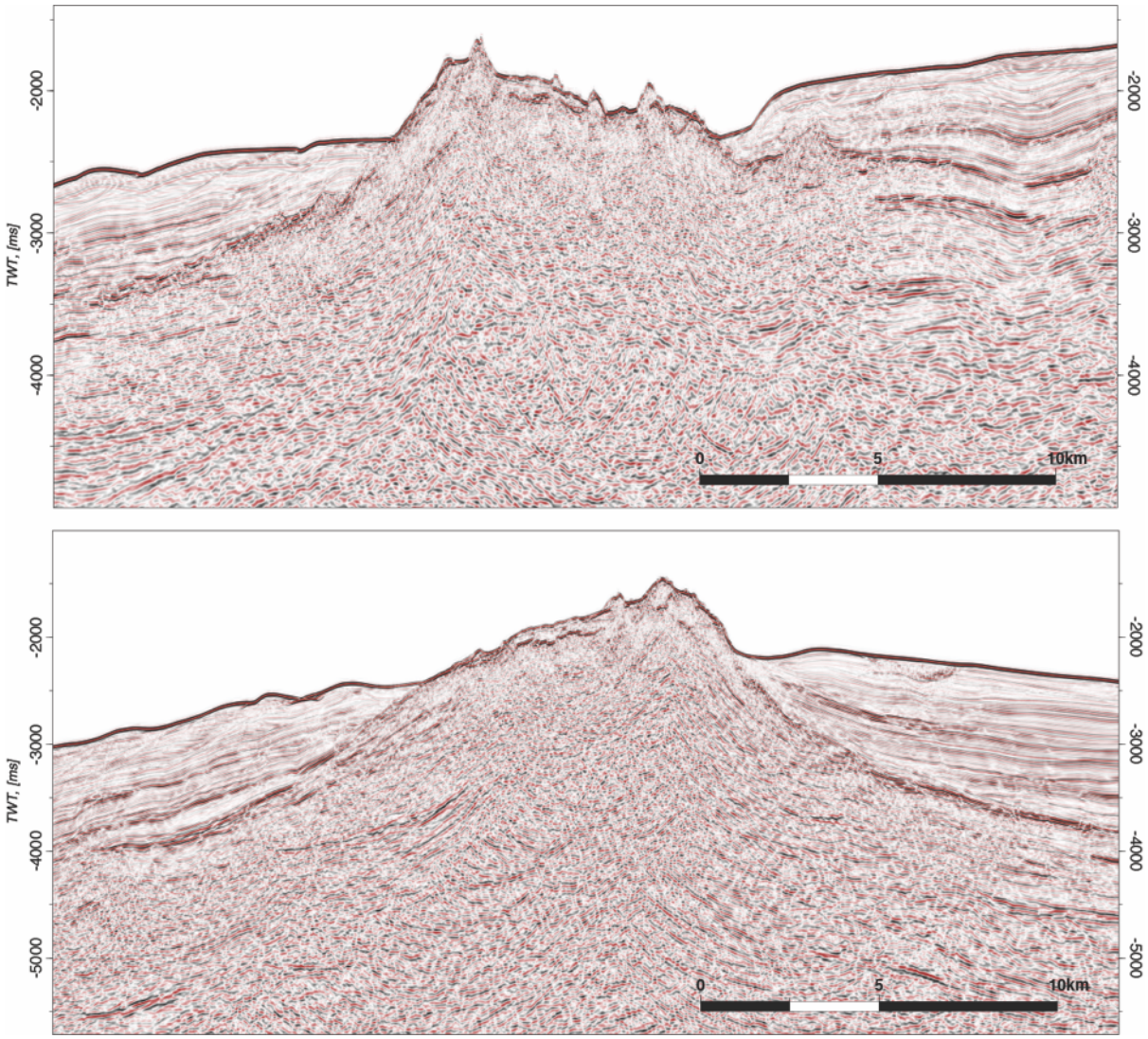

Figure 9. TWT seismic lines across the Fontanelas volcano, highlighting the internal structuration and build-up of the volcanic edifice (outward dipping reflectors), lava flows (in purple), associated secondary vents and deep plumbing systems with multiple sills (in red). Possible erosional terraces at the flank of the volcano suggest possible influence of submergence and shallow water conditions.

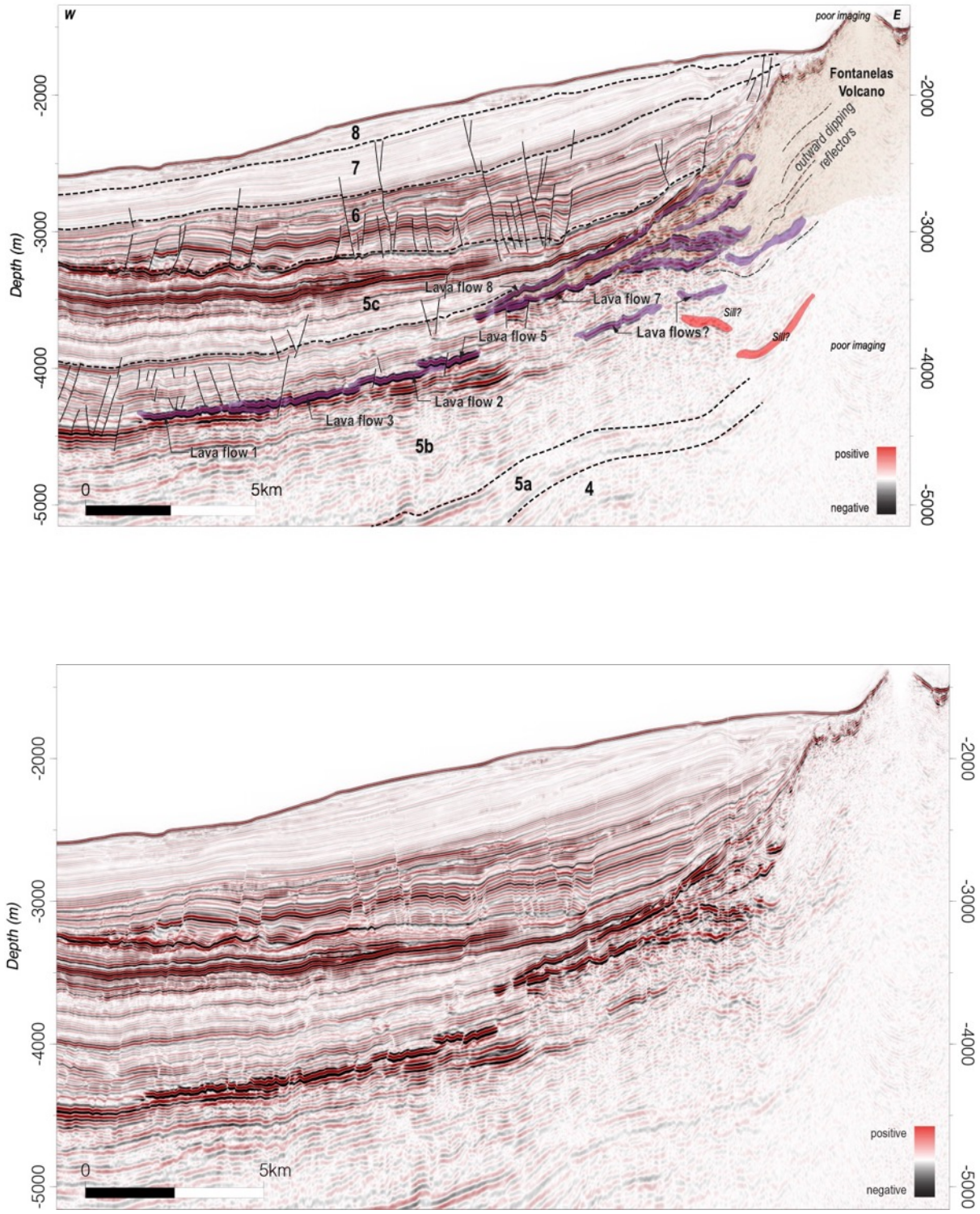

Figure 10. Random seismic line across the southern flank of the volcano, showing pre-Fontanelas lava flows (1 to 5) and syn-Fontanelas lava flows (6-8). See figure 8 for location, figure 11 and Table 1 for details of the lava flows.

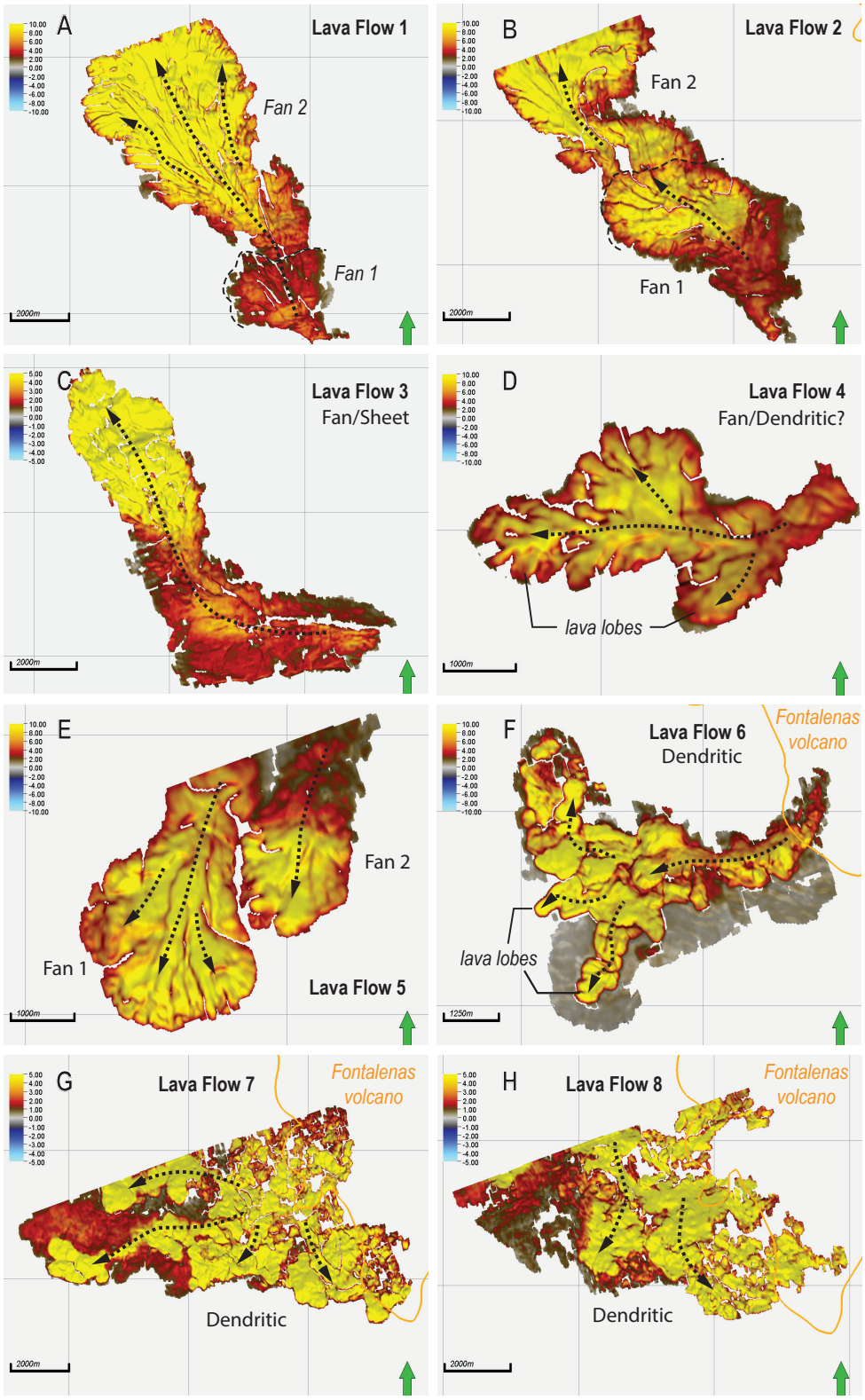

Figure 11. Plan view of seismic amplitudes of interpreted flows, showing multiple lava fans, lobate to crenulated terminations. Arrows indicate likely direction of flow, in relation to its interpreted source and the position of the Fontanelas volcano.

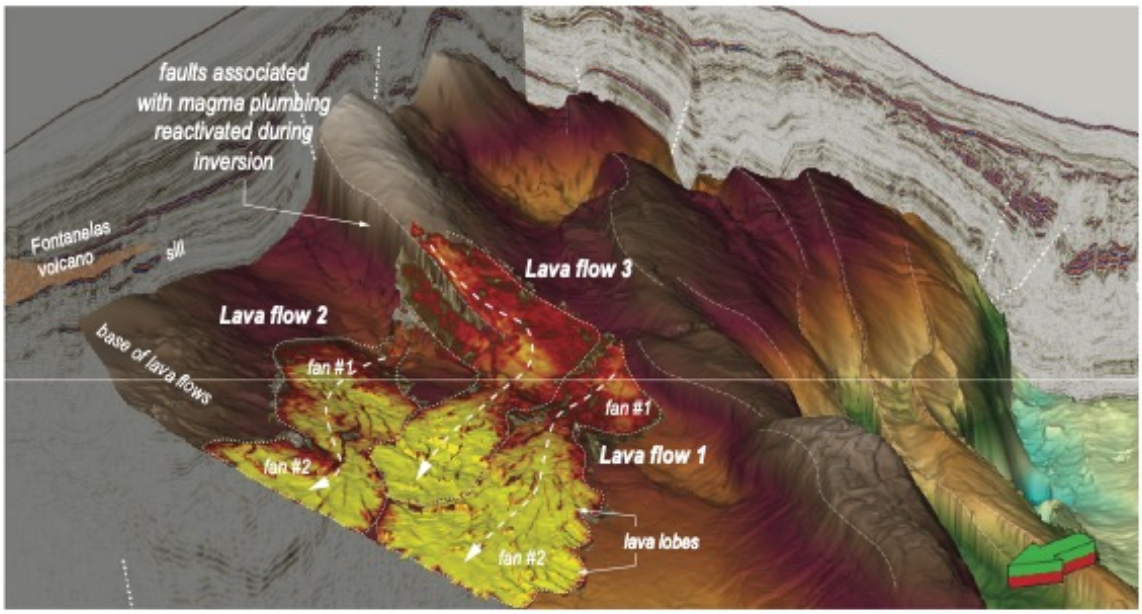

Figure 12. 3D perspective (in depth) of pre-Fontanelas lava flows and interpreted source for fissural magmatism preceding the build-up of the main volcanic edifice. Note the confluence of the origin of lava flows onto inversion faults, likely inherited from the syn-rift architecture.

Nr	Description	Main Direction of Flow	Area (Km^2)	Rock Volume (km3)	Sequence	Relative age
LF1	Lava fans with coalesced lobes	Northwest	37.6	0,87	5b	Pre-Fontanelas
LF2	Lava fans	Northwest	31.1	0,54	5b	Pre-Fontanelas
LF3	Lava sheet/fan(?).	Northwest	28.8	0,95	5b	Pre-Fontanelas
LF4	Possible lava fan with splays and lobes	West	6.8	0,14	5b	Pre-Fontanelas
LF5	Lava fans showing multiple coalesced lobes	South	11.4	0,19	5b	Pre-Fontanelas
LF6	Formed by individual channels of lava, with an overall dendritic shape and individual lobes	West	13.7	0,18	5c	Base Fontanelas
LF7	Multiple dendritic lava flows	South/Southwest	46.1	0,69	5c	Base Fontanelas
LF8	Dendritic lava flows	South	26.6	0,20	5c	Intra-Fontanelas